Supplementary Information for

Thermally induced structural transformations of linear coordination polymers based on aluminum tris(diorganophosphates)

Maciej Dębowski,*[a] Krzysztof Łokaj,[a] Andrzej Ostrowski,[a] Janusz Zachara,[a] Paulina Wiecińska,[a] Paweł Falkowski,[a] Anna Krztoń-Maziopa[a] and Zbigniew Florjańczyk[a]

Faculty of Chemistry, Warsaw University of Technology, Noakowskiego 3, 00-664 Warsaw, Poland.

Analysis of VT–XRD data for DnPPAl

Table S1. Cell parameters (*a* and *c*), cell volume (*V*) and radius of a single chain (*r*) calculated from PXRD patterns collected during heating of DnPPAl sample from 25 °C to 205 °C.

T [°C]	*a* [Å]	*c* [Å]	R_{wp}[a]	*V* [Å^3][b]	*r* [Å][c]
		Low-temperature phase			
25	23.667(5)	9.226(1)	6.6	4475.0(20)	13.664(3)
35	23.700(2)	9.232(7)	7.7	4490.5(4)	13.683(1)
45	23.698(2)	9.265(5)	7.9	4506.2(20)	13.682(1)
55	23.754(1)	9.256(2)	8.1	4522.8(11)	13.714(0)
65	23.772(3)	9.271(3)	7.7	4537.0(20)	13.725(2)
75	23.804(1)	9.287(3)	8.4	4557.3(13)	13.743(1)
85	23.851(6)	9.296(1)	7.6	4579.6(20)	13.770(3)
95	23.855(3)	9.320(3)	8.9	4593.3(20)	13.773(2)
105	23.914(4)	9.317(1)	8.8	4614.4(17)	13.807(2)
115	23.916(2)	9.346(1)	8.9	4629.5(7)	13.808(1)
125	23.916(5)	9.346(1)	8.6	4629.7(20)	13.808(3)
135	23.954(5)	9.407(9)	8.7	4674.5(50)	13.830(3)
145	24.033(7)	9.372(3)	8.8	4687.9(30)	13.875(4)
155	24.030(9)	9.435(1)	8.1	4718.3(30)	13.874(5)
165	24.104(9)	9.382(1)	8.2	4720.5(30)	13.916(5)
175	24.119(3)	9.409(15)	8.4	4740.3(14)	13.925(2)
185	Nd	nd	nd	nd	nd
		High-temperature phase			
185	Nd	nd	nd	nd	nd
195	24.693(0)	9.275(1)	7.0	4897.6(7)	14.256(0)
205	24.856(6)	9.205(2)	5.1	4925.1(30)	14.351(3)

[a] weighted-profile *R*-factor calculated with the formula $R_{\mathrm{wp}} = 100\% \times \{\sum_i w_i[y_i(\mathrm{observed}) - y_i(\mathrm{calculated})]^2 \times \{\sum_i w_i[y_i(\mathrm{observed})]^2\}^{-1}\}^{0.5}$. [b] calculated with the formula $V = 0.5 \times 3^{0.5} \times a^2 \times c$. [c] calculated with the formula $r = 3^{-0.5} \times a$.

Table S2. Cell parameters (*a* and *c*), cell volume (*V*) and radius of a single chain (*r*) calculated from PXRD patterns collected during cooling of DnPPAl sample from 205 °C to 25 °C.

T [°C]	*a* [Å]	*c* [Å]	R_{wp} [a]	*V* [Å^3] [b]	*r* [Å] [c]
		High-temperature phase			
205	24.820(2)	9.197(1)	6.6	4906.6(9)	14.330(1)
195	24.726(1)	9.293(1)	7.0	4920.6(5)	14.276(1)
185	24.667(3)	9.380(1)	6.8	4942.7(11)	14.241(2)
		Low-temperature phase			
185	24.091(3)	9.414(4)	6.8	4731.8(12)	13.909(2)
175	24.112(8)	9.403(1)	8.3	4734.2(30)	13.921(5)
165	24.109(2)	9.401(4)	8.4	4732.2(20)	13.919(1)
155	24.053(1)	9.373(1)	7.6	4695.9(8)	13.887(1)
145	24.008(5)	9.359(4)	7.8	4671.7(30)	13.861(3)
135	23.996(3)	9.352(2)	7.7	4663.5(13)	13.854(2)
125	23.947(6)	9.346(8)	7.9	4641.5(40)	13.826(3)
115	23.931(1)	9.336(6)	7.7	4630.2(30)	13.816(1)
105	23.879(8)	9.326(8)	7.9	4605.2(17)	13.787(5)
95	23.858(1)	9.320(1)	7.4	4594.4(6)	13.775(0)
85	23.824(1)	9.299(3)	7.8	4571.0(15)	13.755(0)
75	23.788(3)	9.288(5)	7.5	4551.6(30)	13.734(2)
65	23.778(1)	9.262(1)	7.5	4535.3(7)	13.728(0)
55	23.751(1)	9.244(5)	7.1	4516.0(30)	13.713(1)
45	23.736(4)	9.223(2)	7.4	4500.1(19)	13.704(2)
35	23.695(3)	9.226(4)	7.0	4486.0(20)	13.680(2)
25	23.667(2)	9.215(2)	7.2	4470.1(12)	13.664(1)

[a] weighted-profile *R*-factor calculated with the formula $R_{wp} = 100\% \times \{\sum_i w_i[y_i(\text{observed}) - y_i(\text{calculated})]^2 \times \{\sum_i w_i[y_i(\text{observed})]^2\}^{-1}\}^{0.5}$. [b] calculated with the formula $V = 0.5 \times 3^{0.5} \times a^2 \times c$. [c] calculated with the formula $r = 3^{-0.5} \times a$.

Although either a linear or *n*–order polynomial fit could be used for fitting those experimental data points given in Tables S1 and S2, the linear fit was applied due to its simplicity and a satisfactory level of approximation. The determination coefficients R^2 for the second or third order polynomial fits (data presented in Table S3) were only marginally better than those of the respective linear regressions described by the following equations (in which *T* is expressed in K) fitted by the least–squares method:

for VT–XRD measurements in a heating mode

$$a(T)_{heat} = 22.77(4)\ \text{Å} + 29.9(11) \times 10^{-4}\ (\text{Å K}^{-1})\ T \quad (R^2 = 0.982) \qquad (S1)$$

$$c(T)_{heat} = 8.83(4)\ \text{Å} + 13.3(10) \times 10^{-4}\ (\text{Å K}^{-1})\ T \quad (R^2 = 0.927) \qquad (S2)$$

$$V(T)_{heat} = 3931(15)\ \text{Å}^3 + 1.81(4)\ (\text{Å}^3\ \text{K}^{-1})\ T \quad (R^2 = 0.993) \qquad (S3)$$

for VT–XRD measurements in a cooling mode

$$a(T)_{cool} = 22.79(3)\ \text{Å} + 29.2(9) \times 10^{-4}\ (\text{Å K}^{-1})\ T \quad (R^2 = 0.987) \qquad (S4)$$

$$c(T)_{cool} = 8.83(2)\ \text{Å} + 12.8(4) \times 10^{-4}\ (\text{Å K}^{-1})\ T \quad (R^2 = 0.983) \qquad (S5)$$

$$V(T)_{cool} = 3942(14)\ \text{Å}^3 + 1.76(4)\ (\text{Å}^3\ \text{K}^{-1})\ T \quad (R^2 = 0.994) \qquad (S6)$$

Table S3. Coefficients of the polynomial fit equations for each unit cell parameter[a] (ucp)= $f(T)= p_0 + p_1T + \ldots + p_nT^n$

Unit cell parameter (ucp)	Order of the polynomial fit, *n*	Coefficients of the polynomial fit				Determination coefficient R^2
		p_0	p_1	p_2	p_3	
VT–XRD measurements in a heating mode (from 298.15 K to 448.15 K)						
a	2	23.265	2.7293×10^{-4}	3.6341×10^{-6}	–	0.9844
	3	19.794	2.8696×10^{-2}	-7.3236×10^{-5}	6.8668×10^{-8}	0.9858
c	2	8.7294	1.8634×10^{-3}	-7.2025×10^{-7}	–	0.9278
	3	12.660	-3.0333×10^{-2}	8.6357×10^{-5}	$-7{,}7785 \times 10^{-8}$	0.9363
V	2	4106.1	8.5195×10^{-1}	1.2791×10^{-3}	–	0.9942
	3	4711.6	−4.1072	1.4691×10^{-2}	-1.1981×10^{-5}	0.9943
VT–XRD measurements in a cooling mode (from 458.15 K to 298.15 K)						
a	2	22.921	2.2231×10^{-3}	9.2264×10^{-7}	–	0.9871
	3	27.689	-3.6384×10^{-2}	1.0405×10^{-4}	-9.0906×10^{-8}	0.9903
c	2	8.5812	2.6311×10^{-3}	-1.7838×10^{-6}	–	0.9865
	3	8.3916	4.1669×10^{-3}	-5.8862×10^{-6}	3.6163×10^{-9}	0.9865
V	2	3897.6	1.9995	-3.1650×10^{-4}	–	0.9938
	3	5659.5	−12.267	3.7793×10^{-2}	-3.3593×10^{-5}	0.9950

[a] unit cell parameters consist of the lattice parameters *a* and *c*, as well as unit cell volume *V*.

Table S4. X-ray powder diffraction data for a solid residue obtained after DMPAl thermal decomposition in air at 600 °C.

Index	2ϑ/°	*d* Value/Å	Rel. Intensity
1	16.183	5.47280	100.0%
2	30.956	2.88648	41.6%

Table S5. X-ray powder diffraction data for a solid residue obtained after DEPAl thermal decomposition in air at 600 °C.

Index	2ϑ/°	*d* Value/Å	Rel. Intensity	Index	2ϑ/°	*d* Value/Å	Rel. Intensity
1	11.705	7.55435	4.2%	25	38.194	2.35447	3.4%
2	12.588	7.02614	2.2%	26	39.932	2.25589	1.5%
3	15.048	5.88275	10.7%	27	41.385	2.17997	1.0%
4	16.201	5.46648	100.0%	28	41.766	2.16095	1.4%
5	17.283	5.12675	22.6%	29	42.892	2.10683	4.4%
6	20.105	4.41316	28.7%	30	43.538	2.07702	5.1%
7	20.998	4.22739	2.3%	31	44.316	2.04234	3.7%
8	21.864	4.06188	13.1%	32	45.233	2.00307	1.3%
9	22.481	3.95176	2.4%	33	46.004	1.97126	1.4%
10	23.269	3.81969	13.5%	34	46.342	1.95766	7.2%
11	23.569	3.77178	24.9%	35	46.606	1.94720	3.5%
12	24.270	3.66429	15.4%	36	47.495	1.91281	2.6%
13	25.403	3.50347	25.0%	37	48.245	1.88481	4.0%
14	26.167	3.40277	11.0%	38	49.673	1.83390	1.3%
15	30.976	2.88466	27.9%	39	52.190	1.75123	3.8%
16	31.834	2.80880	23.4%	40	52.689	1.73581	1.4%
17	32.813	2.72721	7.3%	41	53.816	1.70210	1.8%
18	33.594	2.66561	7.0%	42	55.630	1.65080	2.4%
19	33.840	2.64675	8.2%	43	55.977	1.64141	1.5%
20	34.515	2.59654	15.8%	44	56.908	1.61674	1.0%
21	35.381	2.53490	12.7%	45	57.208	1.60897	2.2%
22	35.738	2.51043	4.7%	46	57.412	1.60373	1.7%
23	37.269	2.41071	5.3%	47	58.188	1.58420	1.1%
24	37.521	2.39512	12.8%	48	59.270	1.55782	1.3%

Table S6. X-ray powder diffraction data for a solid residue obtained after DnPPAl thermal decomposition in air at 600 °C.

Index	2ϑ/°	*d* Value/Å	Rel. Intensity	Index	2ϑ/°	*d* Value/Å	Rel. Intensity
1	11.765	7.51589	4.7%	26	37.254	2.41167	3.2%
2	12.627	7.00472	3.3%	27	37.513	2.39562	6.7%
3	15.057	5.87922	13.6%	28	38.162	2.35636	2.1%
4	16.190	5.47019	100.0%	29	39.918	2.25665	0.6%
5	17.285	5.12602	26.5%	30	41.374	2.18052	0.6%
6	20.101	4.41403	21.5%	31	41.779	2.16034	0.9%
7	21.000	4.22686	1.5%	32	42.887	2.10702	2.0%
8	21.857	4.06310	11.8%	33	43.512	2.07821	2.4%
9	22.479	3.95200	2.6%	34	44.310	2.04263	1.7%
10	23.294	3.81553	10.0%	35	45.228	2.00328	1.1%
11	23.581	3.76989	20.7%	36	45.933	1.97416	1.1%
12	24.136	3.68431	5.2%	37	46.328	1.95825	6.1%
13	24.259	3.66592	7.8%	38	46.633	1.94615	2.8%
14	25.395	3.50449	17.3%	39	47.485	1.91318	1.2%
15	26.158	3.40394	8.3%	40	48.219	1.88577	1.6%
16	28.092	3.17382	1.3%	41	49.616	1.83589	0.8%
17	28.722	3.10564	1.0%	42	51.041	1.78794	0.5%
18	30.974	2.88481	23.5%	43	52.188	1.75130	1.5%
19	31.813	2.81058	15.1%	44	52.650	1.73701	1.4%
20	32.786	2.72937	4.0%	45	53.776	1.70327	1.0%
21	33.622	2.66338	3.5%	46	56.812	1.61923	0.9%
22	33.885	2.64334	3.6%	47	57.200	1.60918	1.2%
23	34.502	2.59744	8.2%	48	57.431	1.60324	1.1%
24	35.369	2.53573	10.1%	49	59.213	1.55919	2.5%
25	35.704	2.51274	2.9%				

Table S7. X-ray powder diffraction data for a solid residue obtained after DiPPAl thermal decomposition in air at 600 °C.

Index	2ϑ/°	*d* Value/Å	Rel. Intensity	Index	2ϑ/°	*d* Value/Å	Rel. Intensity
1	11.722	7.54329	5.1%	35	38.904	2.31308	0.8%
2	12.611	7.01381	3.9%	36	39.929	2.25605	1.4%
3	15.079	5.87090	12.8%	37	41.352	2.18162	1.0%
4	16.197	5.46796	100.0%	38	41.794	2.15958	1.3%
5	17.276	5.12886	24.4%	39	42.893	2.10678	3.2%
6	20.095	4.41528	28.0%	40	43.261	2.08968	1.1%
7	20.952	4.23661	4.0%	41	43.538	2.07705	3.7%
8	21.480	4.13348	16.0%	42	44.313	2.04250	2.7%
9	21.881	4.05879	13.1%	43	44.832	2.02006	0.5%
10	22.441	3.95864	4.0%	44	45.231	2.00315	1.3%
11	23.270	3.81949	12.1%	45	45.967	1.97278	1.5%
12	23.586	3.76900	23.8%	46	46.335	1.95796	5.4%
13	24.101	3.68965	5.9%	47	46.673	1.94457	3.2%
14	24.269	3.66448	11.2%	48	47.488	1.91306	2.2%
15	25.401	3.50364	21.7%	49	48.092	1.89045	1.8%
16	26.177	3.40160	10.4%	50	48.231	1.88533	2.6%
17	27.599	3.22939	0.6%	51	49.656	1.83449	0.8%
18	28.083	3.17489	1.5%	52	50.605	1.80232	0.3%
19	28.719	3.10600	1.1%	53	51.067	1.78709	0.7%
20	29.597	3.01583	0.6%	54	52.187	1.75134	2.5%
21	30.961	2.88600	21.1%	55	52.662	1.73665	1.6%
22	31.817	2.81027	17.9%	56	52.825	1.73167	1.2%
23	32.800	2.72827	4.9%	57	53.104	1.72322	0.7%
24	33.635	2.66243	5.5%	58	53.798	1.70264	1.0%
25	33.936	2.63951	7.3%	59	54.361	1.68632	0.3%
26	34.495	2.59798	11.6%	60	54.643	1.67827	0.9%
27	35.380	2.53501	11.3%	61	55.000	1.66823	0.5%
28	35.744	2.50998	4.3%	62	55.565	1.65259	1.5%
29	36.037	2.49028	1.6%	63	55.962	1.64181	1.6%
30	36.626	2.45157	0.6%	64	56.789	1.61984	1.0%
31	37.261	2.41125	3.7%	65	57.185	1.60956	1.7%
32	37.541	2.39390	9.8%	66	57.380	1.60456	1.2%
33	38.176	2.35552	3.0%	67	58.176	1.58449	0.7%
34	38.550	2.33354	1.3%	68	59.277	1.55766	1.5%

Table S8. X-ray powder diffraction data for a solid residue obtained after DBPAl thermal decomposition in air at 600 °C.

Index	2ϑ/°	*d* Value/Å	Rel. Intensity	Index	2ϑ/°	*d* Value/Å	Rel. Intensity
1	7.763	11.37929	5.1%	40	38.488	2.33716	0.9%
2	11.738	7.53313	5.7%	41	38.909	2.31282	0.6%
3	12.630	7.00317	4.1%	42	39.947	2.25508	1.3%
4	15.062	5.87723	12.3%	43	41.361	2.18116	0.8%
5	16.196	5.46839	100.0%	44	41.804	2.15911	0.9%
6	17.261	5.13314	24.2%	45	42.918	2.10558	2.9%
7	20.076	4.41931	28.3%	46	43.325	2.08677	32.5%
8	20.913	4.24425	2.9%	47	43.433	2.08183	13.8%
9	21.833	4.06758	13.1%	48	44.308	2.04273	2.7%
10	22.432	3.96031	3.0%	49	44.404	2.03852	2.8%
11	23.283	3.81745	11.3%	50	45.234	2.00301	1.3%
12	23.578	3.77022	26.1%	51	45.980	1.97223	1.3%
13	24.089	3.69139	5.4%	52	46.348	1.95744	5.0%
14	24.264	3.66520	10.4%	53	46.624	1.94648	2.7%
15	25.405	3.50313	24.2%	54	47.358	1.91804	1.2%
16	25.584	3.47898	41.7%	55	47.487	1.91312	1.7%
17	26.169	3.40262	10.9%	56	48.105	1.88996	1.7%
18	27.582	3.23141	0.4%	57	48.235	1.88517	2.3%
19	28.091	3.17399	1.4%	58	49.663	1.83427	0.8%
20	28.694	3.10859	1.1%	59	50.597	1.80256	0.3%
21	29.580	3.01752	0.5%	60	51.074	1.78685	0.7%
22	30.973	2.88490	20.5%	61	52.171	1.75182	2.7%
23	31.826	2.80945	16.8%	62	52.578	1.73923	23.8%
24	32.811	2.72740	4.4%	63	52.696	1.73561	11.1%
25	33.382	2.68198	1.4%	64	52.893	1.72962	1.4%
26	33.598	2.66528	5.1%	65	53.247	1.71894	0.7%
27	33.889	2.64305	6.1%	66	53.804	1.70245	1.0%
28	34.505	2.59723	10.7%	67	54.357	1.68643	0.2%
29	35.129	2.55256	11.2%	68	54.637	1.67844	0.9%
30	35.236	2.54501	7.8%	69	55.022	1.66760	0.5%
31	35.368	2.53584	8.0%	70	55.529	1.65358	1.3%
32	35.704	2.51271	3.5%	71	55.896	1.64358	1.2%
33	36.000	2.49277	1.1%	72	56.080	1.63863	1.4%
34	36.622	2.45185	0.5%	73	56.762	1.62055	1.0%
35	37.257	2.41145	4.4%	74	57.168	1.60999	2.2%
36	37.545	2.39367	10.3%	75	57.641	1.59792	7.2%
37	37.808	2.37761	25.5%	76	57.501	1.60146	12.8%
38	37.895	2.37234	10.5%	77	58.169	1.58465	0.6%
39	38.169	2.35593	2.7%	78	59.254	1.55820	1.7%

Table S9. X-ray powder diffraction data for a solid residue obtained after BEHPAl thermal decomposition in air at 600 °C.

Index	2ϑ/°	*d* Value/Å	Rel. Intensity	Index	2ϑ/°	*d* Value/Å	Rel. Intensity
1	11.695	7.56108	4.3%	36	36.578	2.45466	0.6%
2	12.601	7.01934	4.2%	37	37.222	2.41369	4.5%
3	15.042	5.88511	12.5%	38	37.525	2.39485	11.7%
4	15.775	5.61337	2.8%	39	38.175	2.35558	5.4%
5	16.193	5.46942	100.0%	40	38.532	2.33457	1.3%
6	17.272	5.13005	26.5%	41	38.889	2.31393	0.6%
7	18.256	4.85576	1.0%	42	39.925	2.25625	1.6%
8	20.092	4.41597	29.6%	43	40.458	2.22778	1.2%
9	20.388	4.35243	9.8%	44	41.472	2.17558	1.3%
10	20.944	4.23808	3.5%	45	41.779	2.16033	1.8%
11	21.456	4.13820	20.7%	46	42.882	2.10727	3.6%
12	21.806	4.07254	12.2%	47	43.545	2.07670	4.5%
13	22.436	3.95952	3.5%	48	44.314	2.04246	3.0%
14	23.237	3.82484	13.1%	49	45.233	2.00305	1.3%
15	23.584	3.76927	26.1%	50	45.920	1.97469	1.7%
16	24.246	3.66789	15.5%	51	46.338	1.95784	5.9%
17	25.399	3.50400	24.7%	52	46.627	1.94636	3.7%
18	25.929	3.43357	7.2%	53	47.493	1.91290	2.3%
19	26.156	3.40418	12.4%	54	48.229	1.88539	2.9%
20	27.581	3.23146	0.6%	55	48.644	1.87029	1.1%
21	28.122	3.17058	1.7%	56	49.651	1.83468	1.2%
22	28.744	3.10335	1.1%	57	51.057	1.78741	0.7%
23	29.019	3.07457	2.4%	58	52.219	1.75034	3.1%
24	29.571	3.01844	0.8%	59	52.575	1.73933	2.2%
25	30.532	2.92555	4.4%	60	53.789	1.70288	1.2%
26	30.958	2.88625	24.4%	61	54.651	1.67804	0.9%
27	31.814	2.81056	21.4%	62	55.073	1.66619	1.0%
28	32.797	2.72851	5.9%	63	55.679	1.64947	1.6%
29	33.301	2.68835	2.1%	64	55.940	1.64240	2.3%
30	33.615	2.66393	5.8%	65	56.884	1.61736	1.6%
31	33.888	2.64310	7.9%	66	57.175	1.60982	2.1%
32	34.490	2.59834	13.8%	67	57.555	1.60008	1.4%
33	35.370	2.53569	13.1%	68	58.148	1.58518	0.8%
34	35.696	2.51329	5.5%	69	59.283	1.55750	1.9%
35	36.040	2.49009	2.0%				

Table S10. X-ray powder diffraction data for a solid residue obtained after BEHPAl thermal decomposition (6 h) in argon atmosphere at 600 °C.

Index	2ϑ/°	*d* Value/Å	Rel. Intensity	Index	2ϑ/°	*d* Value/Å	Rel. Intensity
1	11.738	7.53310	4.7%	34	38.156	2.35672	15.8%
2	12.631	7.00238	3.6%	35	38.531	2.33465	1.6%
3	15.048	5.88281	12.8%	36	38.942	2.31090	0.8%
4	15.788	5.60883	12.3%	37	39.929	2.25605	1.7%
5	16.182	5.47309	100.0%	38	40.437	2.22884	9.9%
6	17.273	5.12961	24.0%	39	41.546	2.17190	6.3%
7	18.229	4.86272	5.8%	40	42.594	2.12086	2.8%
8	20.087	4.41702	28.0%	41	42.810	2.11064	4.1%
9	20.397	4.35046	55.5%	42	43.522	2.07776	5.2%
10	20.896	4.24781	3.0%	43	44.294	2.04334	3.4%
11	21.442	4.14083	21.8%	44	44.763	2.02301	0.5%
12	21.858	4.06294	14.9%	45	45.196	2.00460	1.4%
13	22.433	3.96003	3.2%	46	45.782	1.98031	4.0%
14	23.243	3.82385	14.3%	47	46.345	1.95757	7.4%
15	23.567	3.77207	22.3%	48	46.646	1.94561	7.3%
16	24.220	3.67181	41.8%	49	47.481	1.91334	2.9%
17	25.386	3.50577	23.5%	50	47.728	1.90401	2.6%
18	25.923	3.43436	41.2%	51	48.226	1.88549	3.3%
19	26.150	3.40505	13.2%	52	48.665	1.86950	9.7%
20	28.087	3.17439	1.6%	53	49.616	1.83590	2.4%
21	29.027	3.07368	16.6%	54	51.051	1.78761	0.9%
22	29.523	3.02319	0.6%	55	52.403	1.74463	7.4%
23	30.488	2.92969	28.0%	56	52.834	1.73138	2.0%
24	30.943	2.88764	26.6%	57	53.773	1.70336	1.4%
25	31.800	2.81175	23.8%	58	54.258	1.68926	0.6%
26	32.801	2.72821	6.5%	59	54.661	1.67778	0.6%
27	33.225	2.69433	17.2%	60	55.088	1.66578	6.9%
28	33.851	2.64591	7.5%	61	55.635	1.65068	2.3%
29	34.471	2.59974	15.0%	62	55.935	1.64252	5.1%
30	35.356	2.53666	15.0%	63	56.848	1.61831	6.7%
31	35.713	2.51214	10.7%	64	57.672	1.59713	10.5%
32	36.554	2.45626	0.6%	65	59.291	1.55732	2.4%
33	37.499	2.39649	12.1%	66			

Table S11. X-ray powder diffraction data for a solid residue obtained after BEHPAl thermal decomposition (24 h) in argon atmosphere at 600 °C.

Index	2ϑ/°	*d* Value/Å	Rel. Intensity	Index	2ϑ/°	*d* Value/Å	Rel. Intensity
1	11.719	7.54553	5.0%	38	37.523	2.39497	14.0%
2	12.635	7.00018	4.0%	39	38.174	2.35565	11.7%
3	15.052	5.88114	11.7%	40	38.456	2.33903	2.2%
4	15.799	5.60464	7.1%	41	38.956	2.31012	1.3%
5	16.189	5.47080	100.0%	42	39.932	2.25587	1.9%
6	17.280	5.12754	26.1%	43	40.448	2.22831	5.9%
7	18.237	4.86069	3.3%	44	41.569	2.17073	4.1%
8	20.088	4.41666	31.7%	45	42.854	2.10859	5.1%
9	20.422	4.34523	35.1%	46	43.247	2.09035	1.6%
10	20.965	4.23389	3.4%	47	43.534	2.07721	6.1%
11	21.463	4.13677	26.3%	48	44.301	2.04299	4.0%
12	21.791	4.07531	13.1%	49	44.715	2.02506	0.7%
13	22.439	3.95894	3.7%	50	45.217	2.00374	2.1%
14	23.277	3.81839	12.5%	51	45.830	1.97833	3.5%
15	23.575	3.77077	26.2%	52	46.341	1.95773	8.1%
16	24.233	3.66986	29.3%	53	46.636	1.94601	6.5%
17	25.404	3.50324	24.7%	54	47.520	1.91186	3.7%
18	25.906	3.43649	24.3%	55	48.223	1.88560	4.4%
19	26.163	3.40329	13.3%	56	48.667	1.86945	5.9%
20	27.616	3.22752	0.9%	57	49.641	1.83503	2.2%
21	28.064	3.17702	1.8%	58	51.048	1.78771	1.0%
22	28.685	3.10960	1.5%	59	52.165	1.75203	4.6%
23	29.034	3.07299	10.0%	60	52.389	1.74506	5.2%
24	29.544	3.02109	0.7%	61	52.860	1.73060	2.2%
25	30.499	2.92865	16.1%	62	53.200	1.72034	1.1%
26	30.958	2.88624	27.0%	63	53.779	1.70318	1.8%
27	31.817	2.81028	24.3%	64	54.287	1.68844	0.5%
28	32.803	2.72800	6.9%	65	54.622	1.67887	1.5%
29	33.251	2.69227	9.6%	66	55.100	1.66544	4.3%
30	33.557	2.66839	7.0%	67	55.580	1.65217	2.5%
31	33.873	2.64422	9.7%	68	55.935	1.64254	4.6%
32	34.491	2.59829	16.2%	69	56.817	1.61912	4.6%
33	35.363	2.53620	16.5%	70	57.110	1.61149	3.3%
34	35.692	2.51355	9.1%	71	57.663	1.59736	6.6%
35	36.045	2.48972	2.6%	72	58.069	1.58714	1.3%
36	36.603	2.45307	0.6%	73	59.212	1.55920	3.0%
37	37.226	2.41343	5.9%	74			

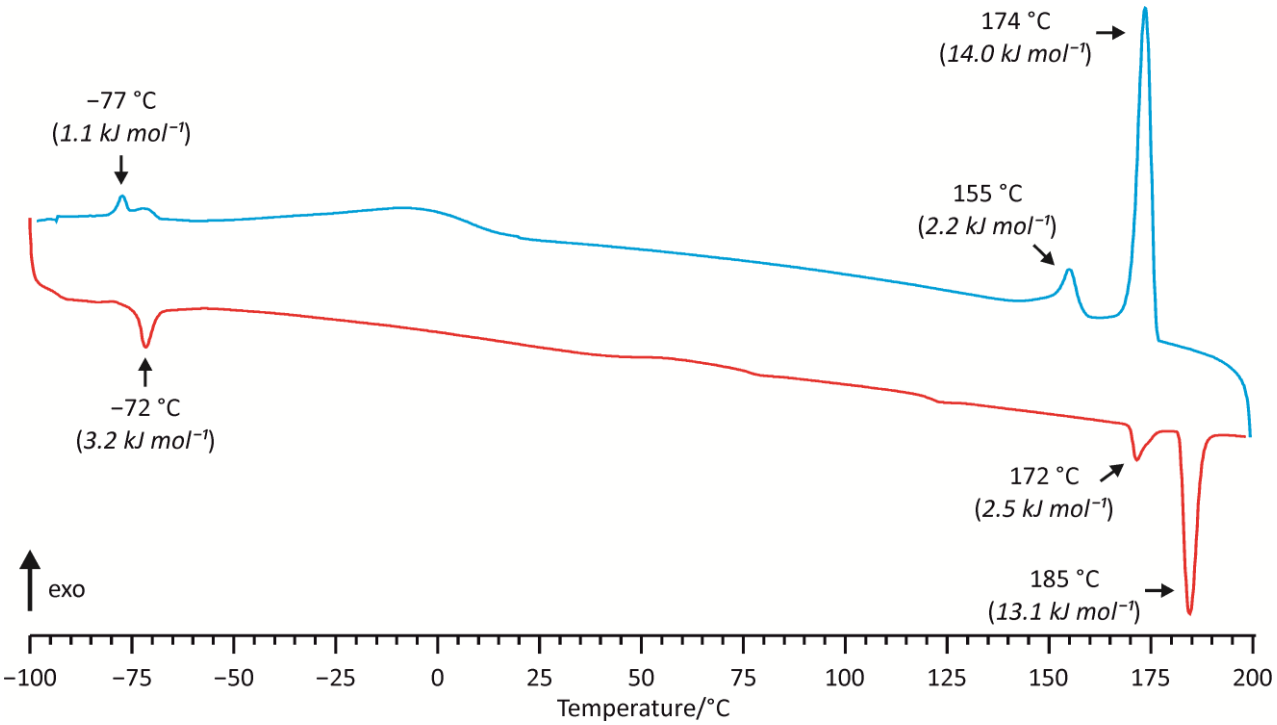

Figure S1. DSC trace of DnPPAl. The 1st heating (red) and cooling (blue) curves are presented. Enthalpies of the first-order transitions are given in parentheses.

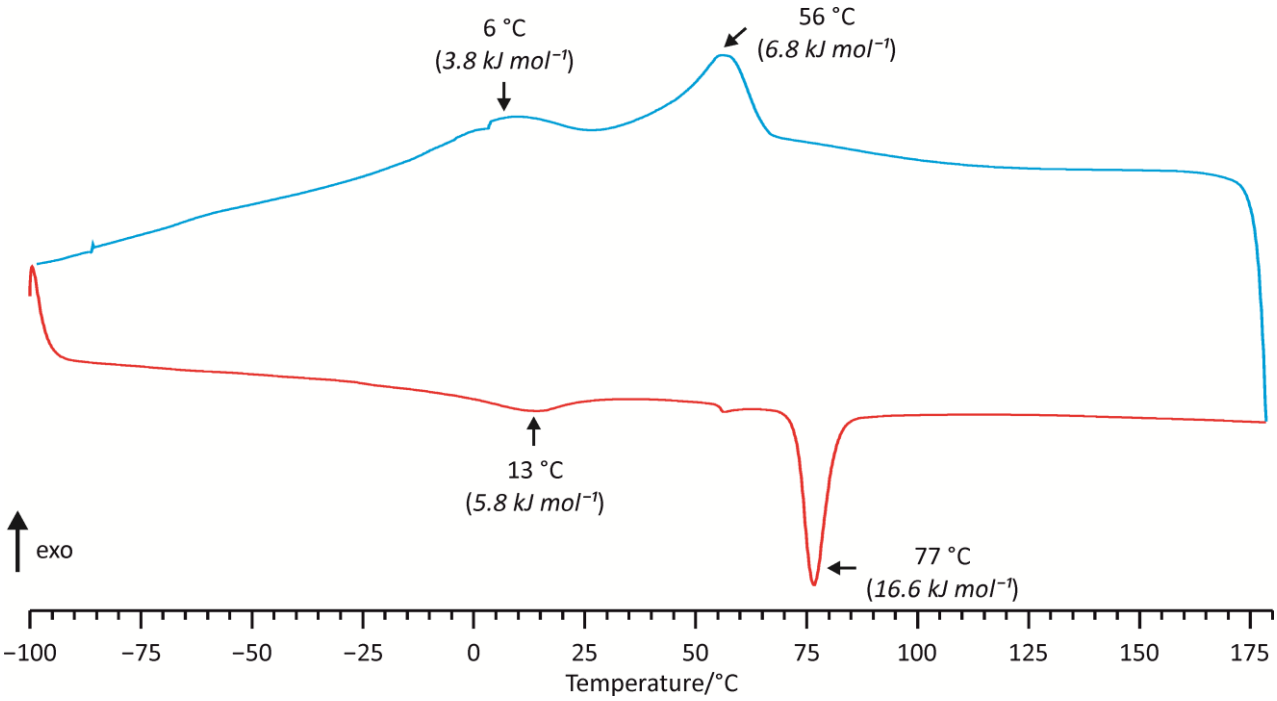

Figure S2. DSC trace of DBPAl. The 1st heating (red) and cooling (blue) curves are presented. Enthalpies of the first-order transitions are given in parentheses.

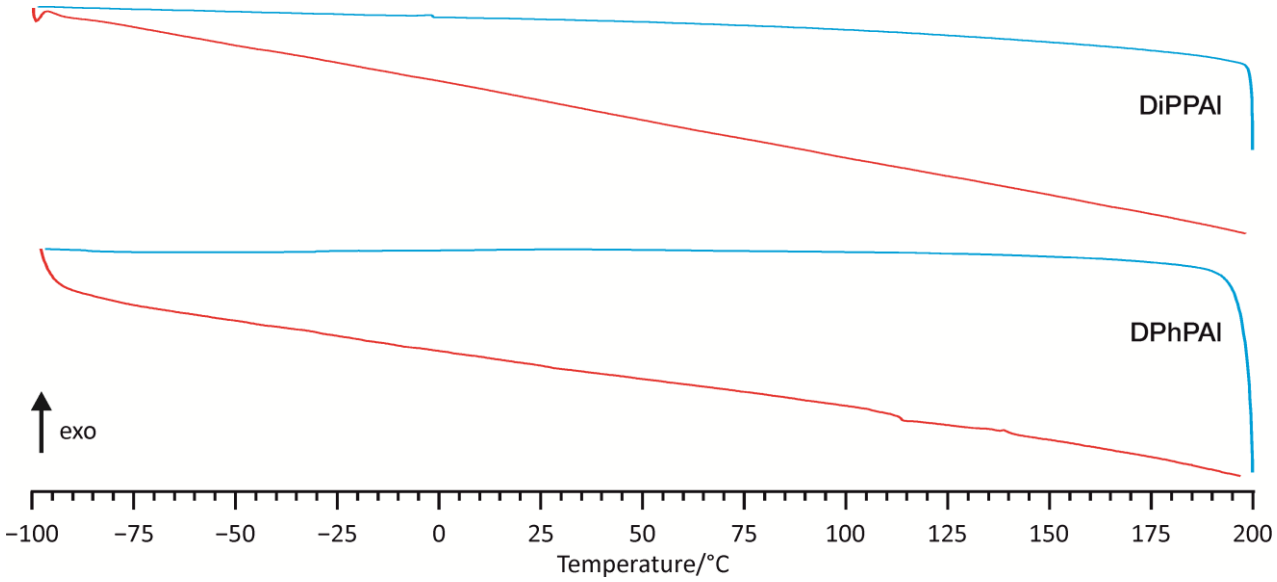

Figure S3. DSC traces of DiPPAl (top) and DPhPAl (bottom). The 1st heating (red) and cooling (blue) curves are presented.

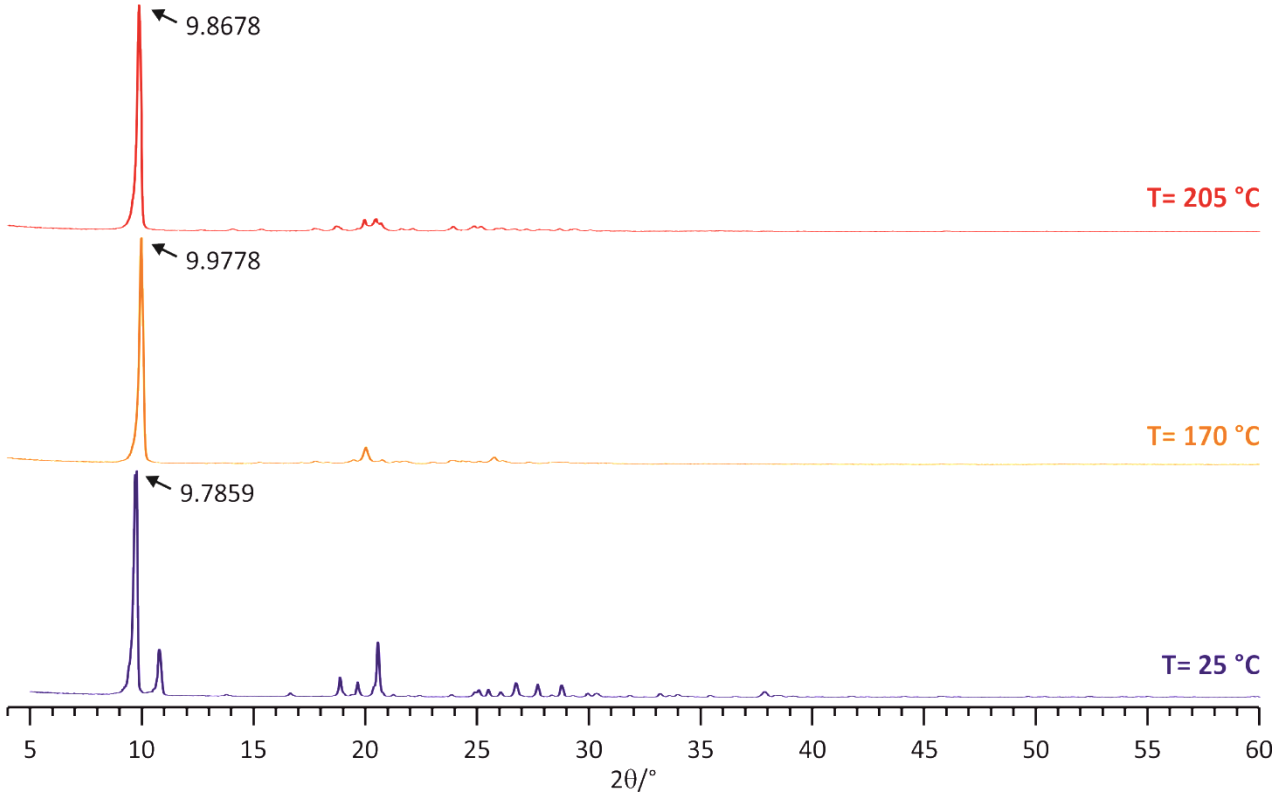

Figure S4. PXRD patterns of DMPAl measured at 25 °C (bottom), 170 °C (middle) and 205 °C (top).

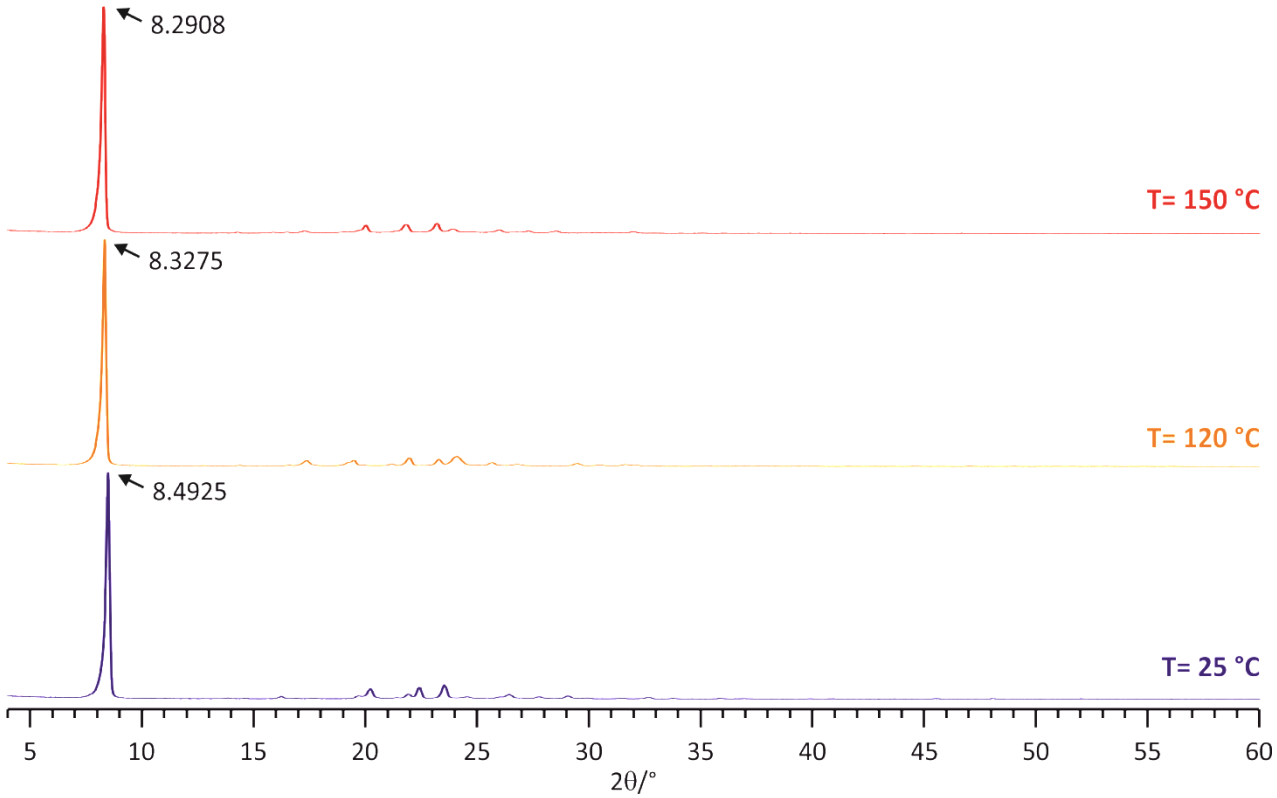

Figure S5. PXRD patterns of DEPAl measured at 25 °C (bottom), 120 °C (middle) and 150 °C (top).

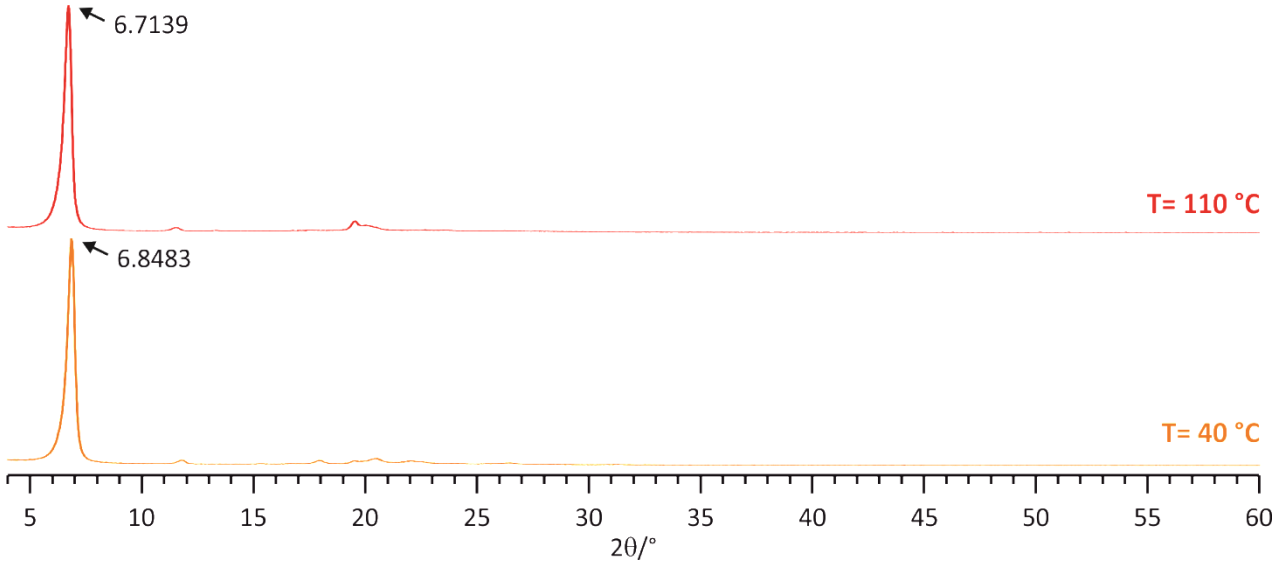

Figure S6. PXRD patterns of DBPAl measured at 40°C (bottom) and 110 °C (top).

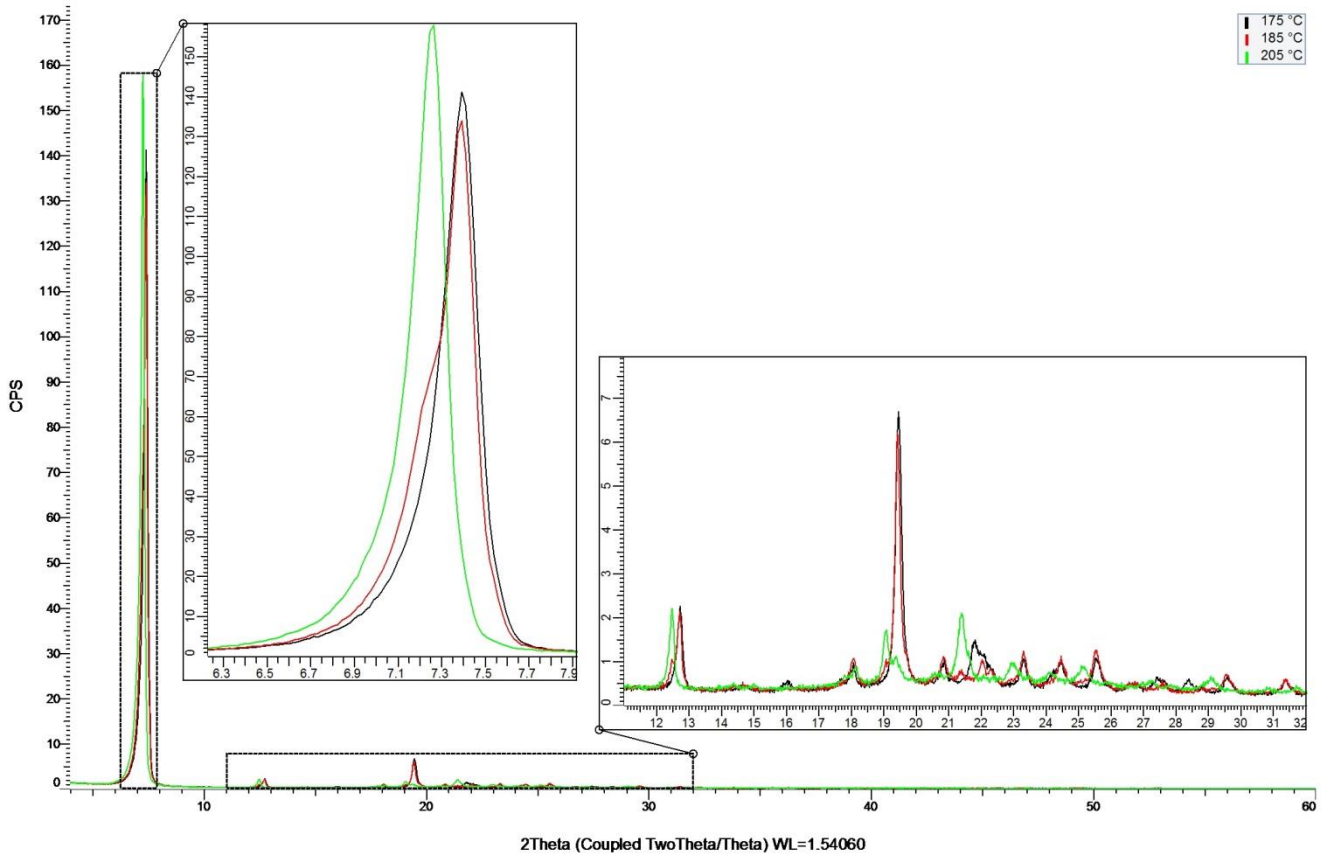

Figure S7. VT–PXRD patterns of DnPPAl measured in a heating mode (from 25 °C to 205 °C) at temperature of: 175 °C (black line), 185 °C (red line) and 205 °C (green line).

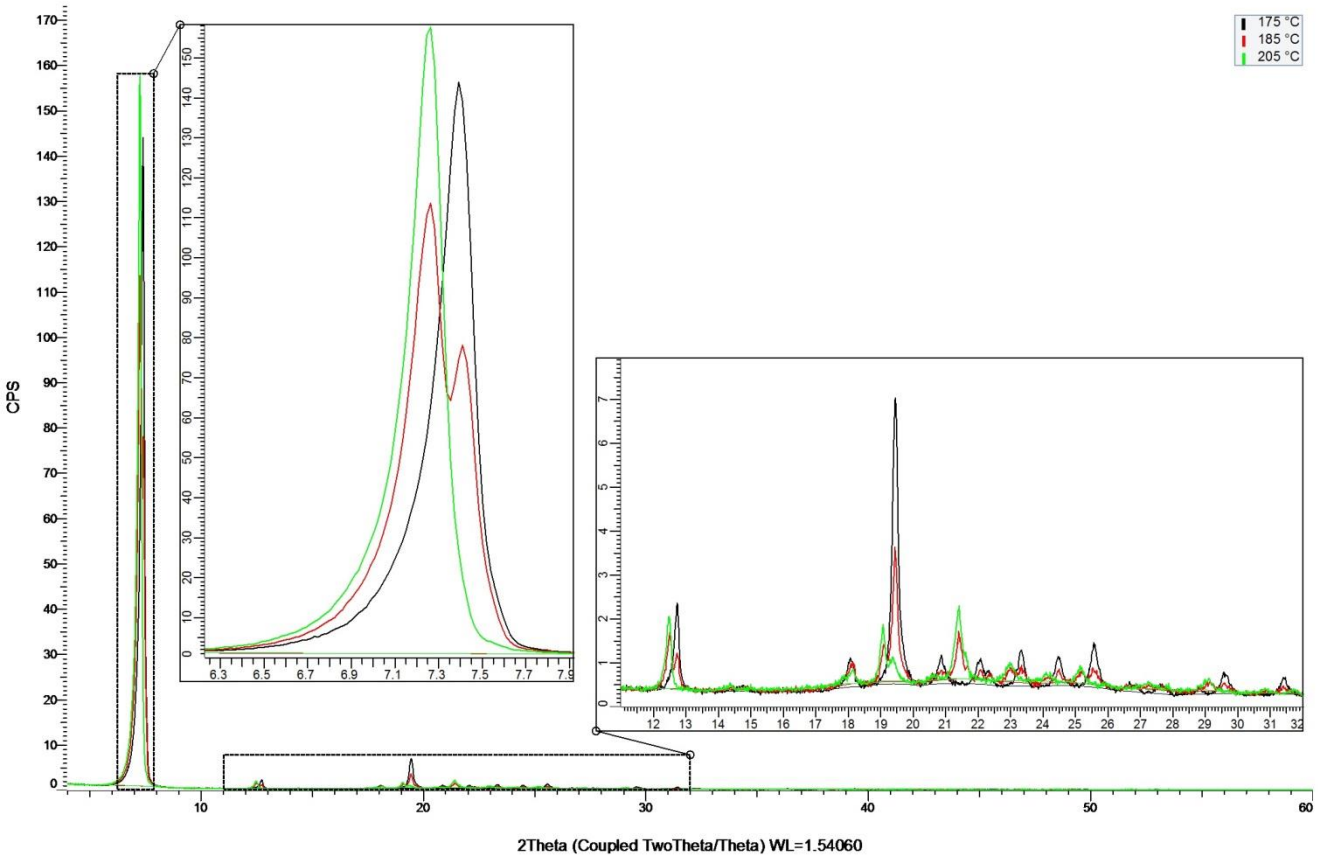

Figure S8. VT–PXRD patterns of DnPPAl measured in a cooling mode (from 205 °C to 25 °C) at temperature of: 175 °C (black line), 185 °C (red line) and 205 °C (green line).

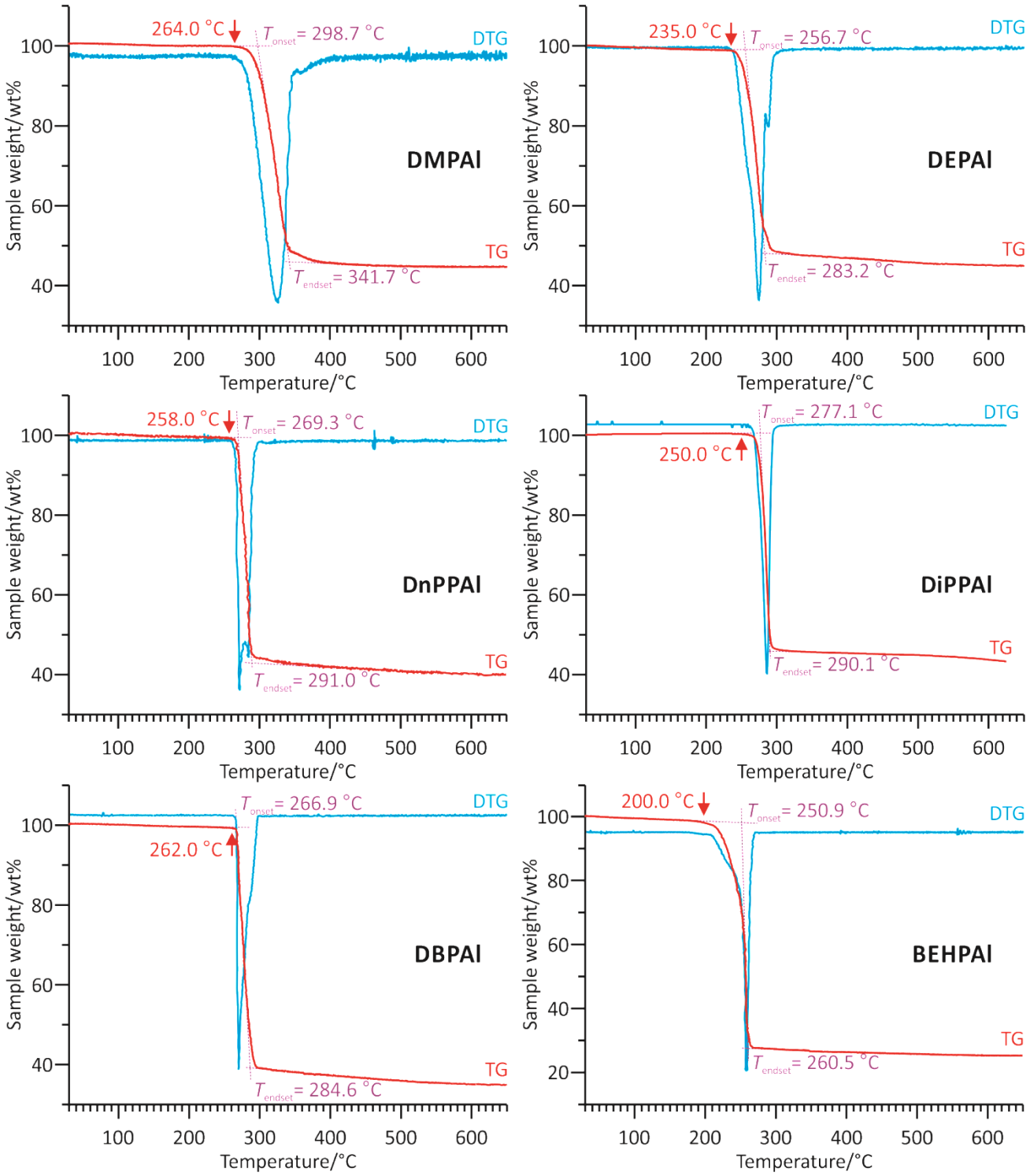

Figure S9. TG (red lines) and DTG (blue lines) profiles of DOPAl containing aliphatic groups. The measurements were carried out in air at a heating rate of 10 °C min^{-1}. T_{onset} and T_{endset} denote the extrapolated onset and endset temperatures derived from the intersection of two tangents (purple, dashed lines), respectively. The red arrows indicate temperature of the beginning of weight loss (bend point on the TG curve).

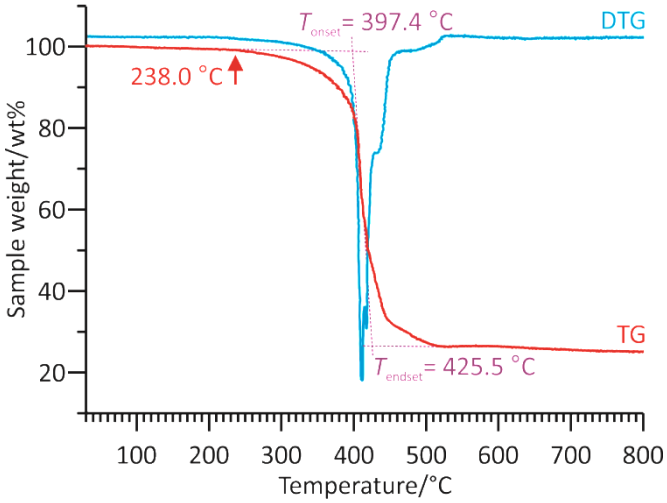

Figure S10. TG (red line) and DTG (blue line) profiles of DPhPAl. The measurements were carried out in air at a heating rate of 10 °C min^{-1}. T_{onset} and T_{endset} denote the extrapolated onset and endset temperature derived from the intersection of two tangents (purple, dashed lines), respectively. The red arrow indicates temperature of the beginning of weight loss (bend point on the TG curve).

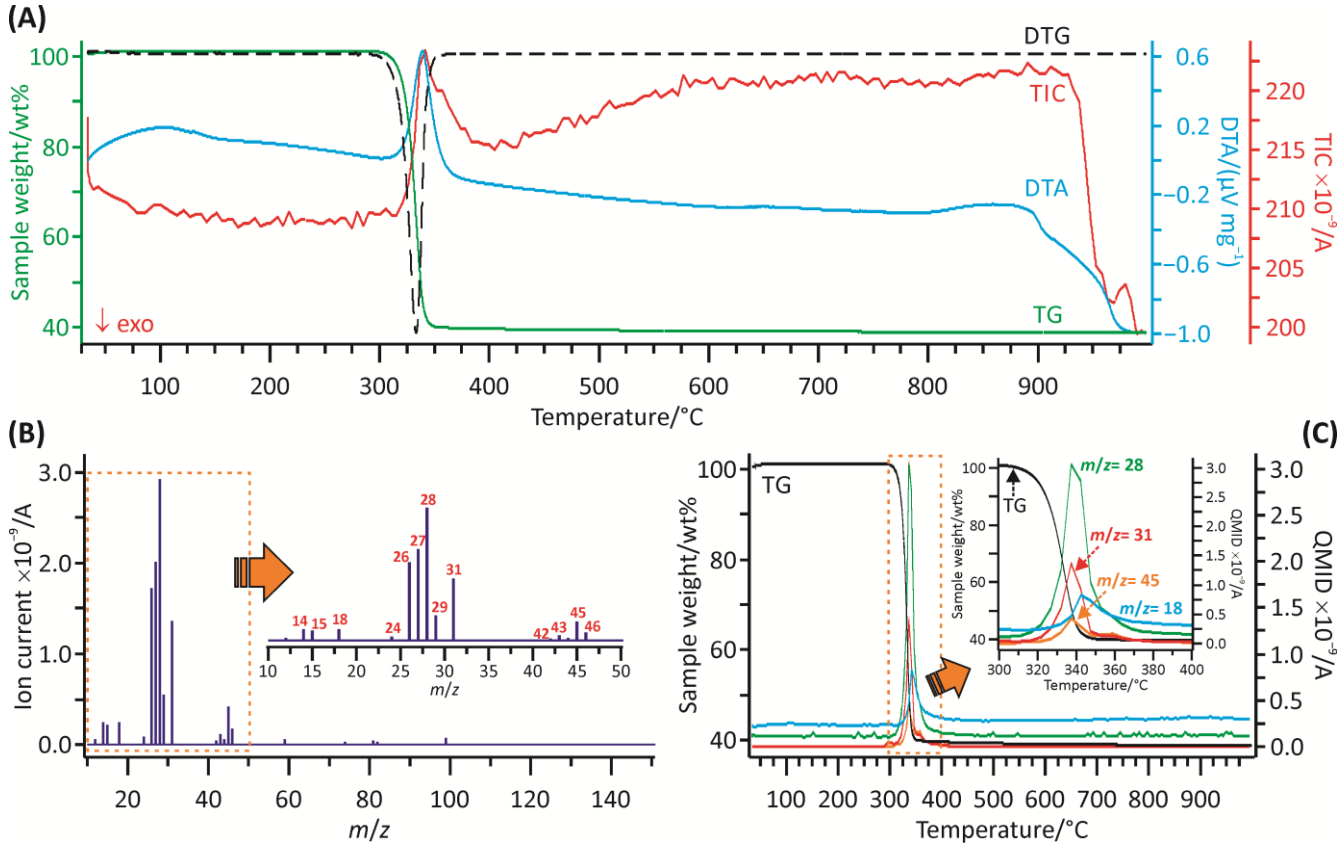

Figure S11. Thermogravimetric (TG) analysis of DEPAl coupled with differential thermal analysis (DTA) and quadrupole mass spectrometry (QMS) of the evolved gas: (A) TG, DTG, DTA and Total Ion Current (TIC) profiles, (B) QMS spectrum of the evolved gas obtained at temperature of 337.3 °C, (C) TG profile (black line) and QMS curves (colored lines) for the ions characteristic for: ethylene (m/z = 28), ethanol (m/z = 31, 45) and water (m/z = 18).

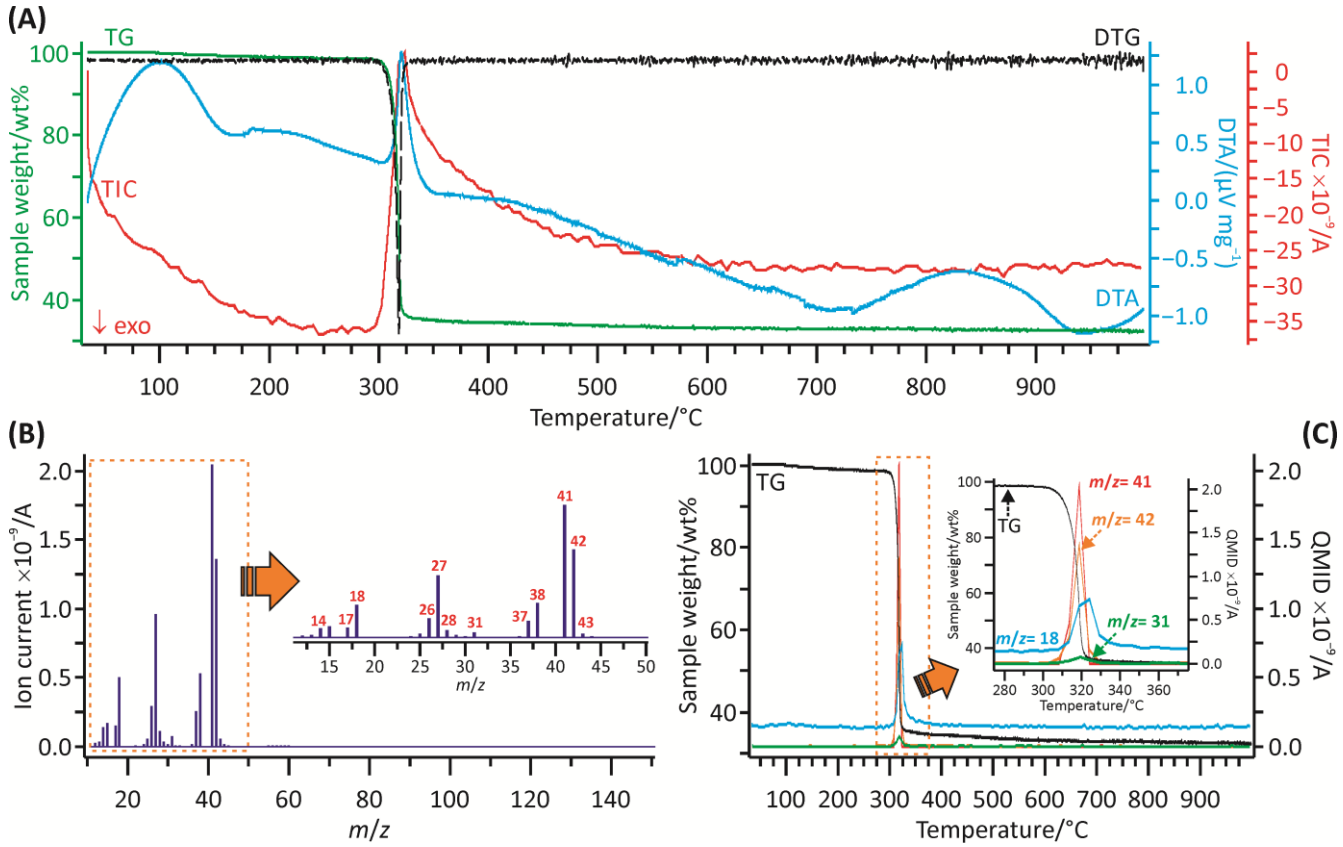

Figure S12. Thermogravimetric (TG) analysis of DnPPAl coupled with differential thermal analysis (DTA) and quadrupole mass spectrometry (QMS) of the evolved gas: (A) TG, DTG, DTA and Total Ion Current (TIC) profiles, (B) QMS spectrum of the evolved gas obtained at temperature of 318.8 °C, (C) TG profile (black line) and QMS curves (colored lines) for the ions characteristic for: propene (*m*/*z* = 41, 42), 1-propanol (*m*/*z* = 31) and water (*m*/*z* = 18).

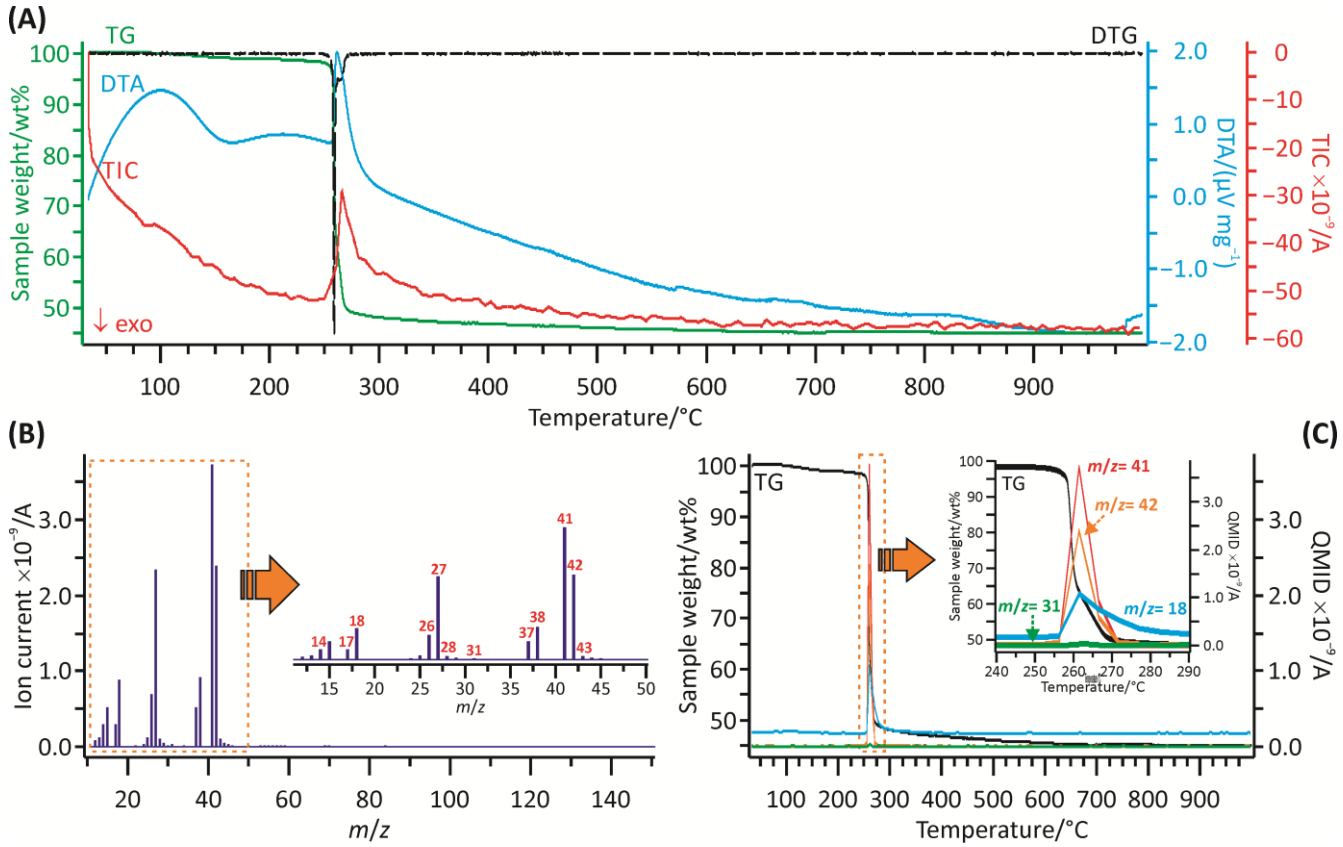

Figure S13. Thermogravimetric (TG) analysis of DiPPAl coupled with differential thermal analysis (DTA) and quadrupole mass spectrometry (QMS) of the evolved gas: (A) TG, DTG, DTA and Total Ion Current (TIC) profiles, (B) QMS spectrum of the evolved gas obtained at temperature of 261.5 °C, (C) TG profile (black line) and QMS curves for the ions characteristic for: propene (*m*/*z* = 41, 42), 2-propanol (*m*/*z* = 31) and water (*m*/*z* = 18).

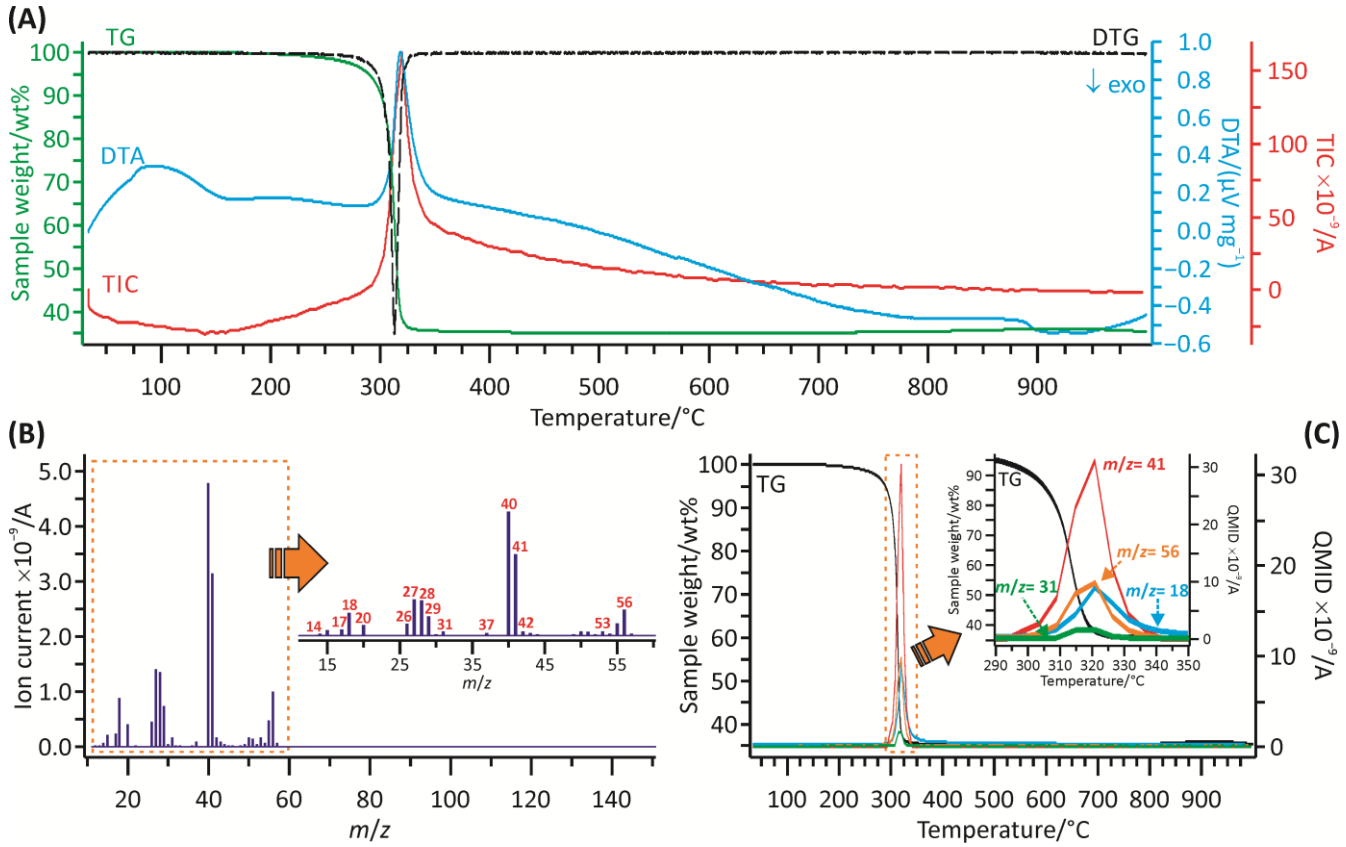

Figure S14. Thermogravimetric (TG) analysis of DBPAl coupled with differential thermal analysis (DTA) and quadrupole mass spectrometry (QMS) of the evolved gas: (A) TG, DTG, DTA and Total Ion Current (TIC) profiles, (B) QMS spectrum of the evolved gas obtained at temperature of 320.8 °C, (C) TG profile (black line) and QMS curves for the ions characteristic for: isomers of butene (*m*/*z* = 41, 56), 1-butanol (*m*/*z* = 31) and water (*m*/*z* = 18).

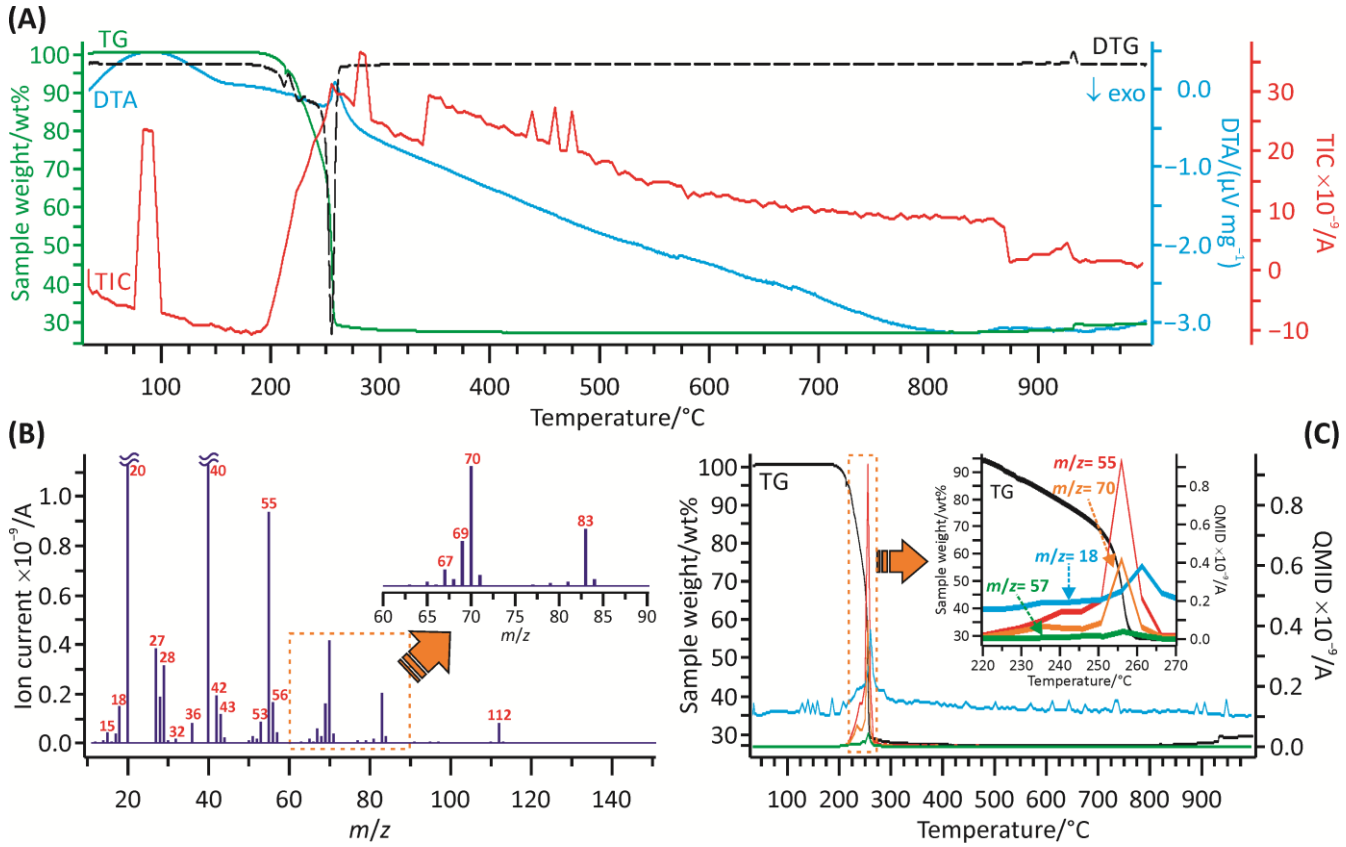

Figure S15. Thermogravimetric (TG) analysis of BEHPAl coupled with differential thermal analysis (DTA) and quadrupole mass spectrometry (QMS) of the evolved gas: (A) TG, DTG, DTA and Total Ion Current (TIC) profiles, (B) QMS spectrum of the evolved gas obtained at temperature of 256.0 °C, (C) TG profile (black line) and QMS curves for the ions characteristic for: 2-ethyl-1-hexene (*m/z* = 55, 70), 2-ethyl-1-hexanol (*m/z* = 57) and water (*m/z* = 18).

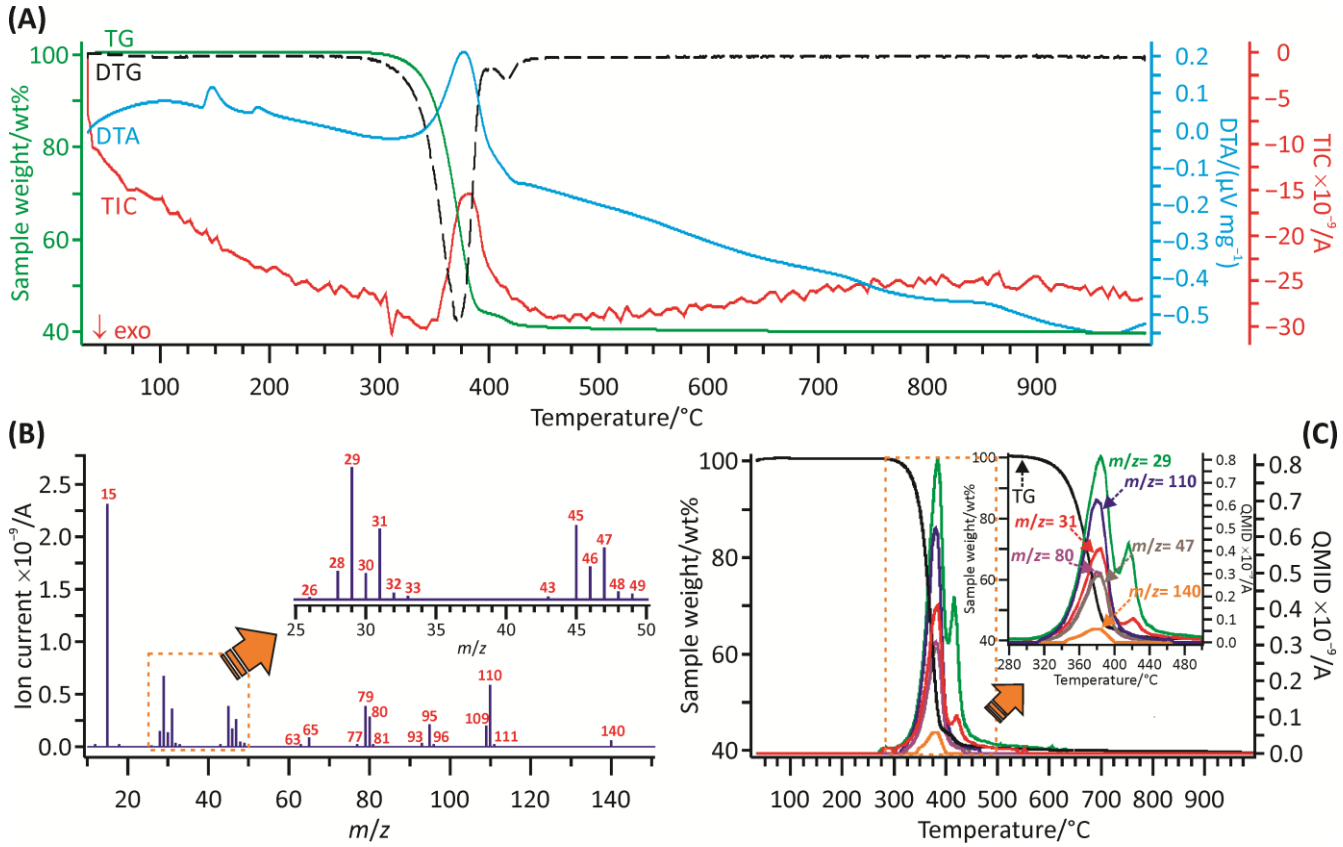

Figure S16. Thermogravimetric (TG) analysis of DMPAl coupled with differential thermal analysis (DTA) and quadrupole mass spectrometry (QMS) of the evolved gas: (A) TG, DTG, DTA and Total Ion Current (TIC) profiles, (B) QMS spectrum of the evolved gas obtained at temperature of 374.3 °C, (C) TG profile (black line) and QMS curves for the ions characteristic for: dimethyl ether (*m/z* = 29), methanol (*m/z* = 31), PO group (*m/z* = 47), $HOPO_2$ group (*m/z* = 80), dimethylphosphite (*m/z* = 110) and trimethyl phosphate molecular ion (*m/z* = 140)

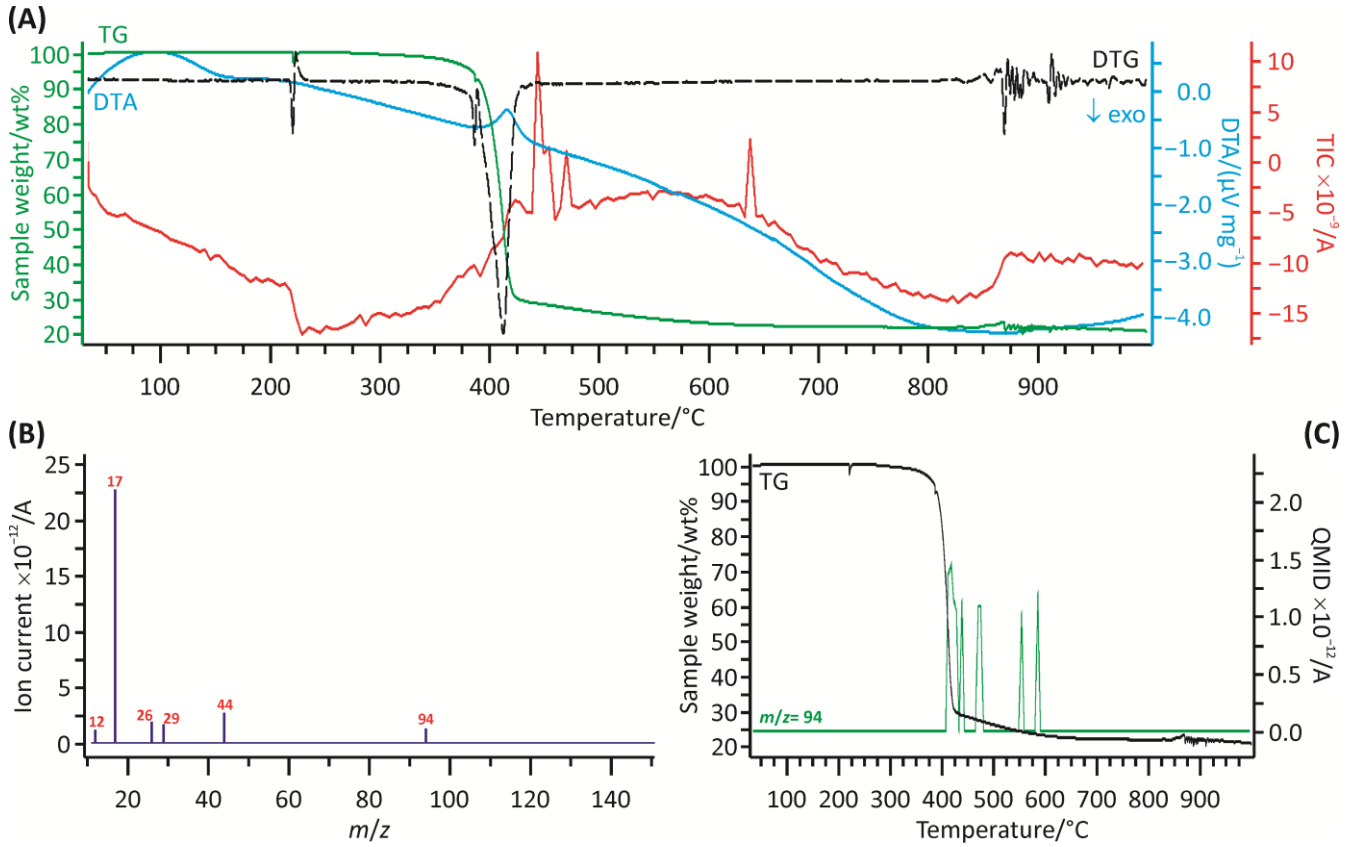

Figure S17. Thermogravimetric (TG) analysis of DPhPAl coupled with differential thermal analysis (DTA) and quadrupole mass spectrometry (QMS) of the evolved gas: (A) TG, DTG, DTA and Total Ion Current (TIC) profiles, (B) QMS spectrum of the evolved gas obtained at temperature of 412.8 °C, (C) TG profile (black line) and QMS curve (green line) for the ion with *m*/*z*= 94 (phenol).

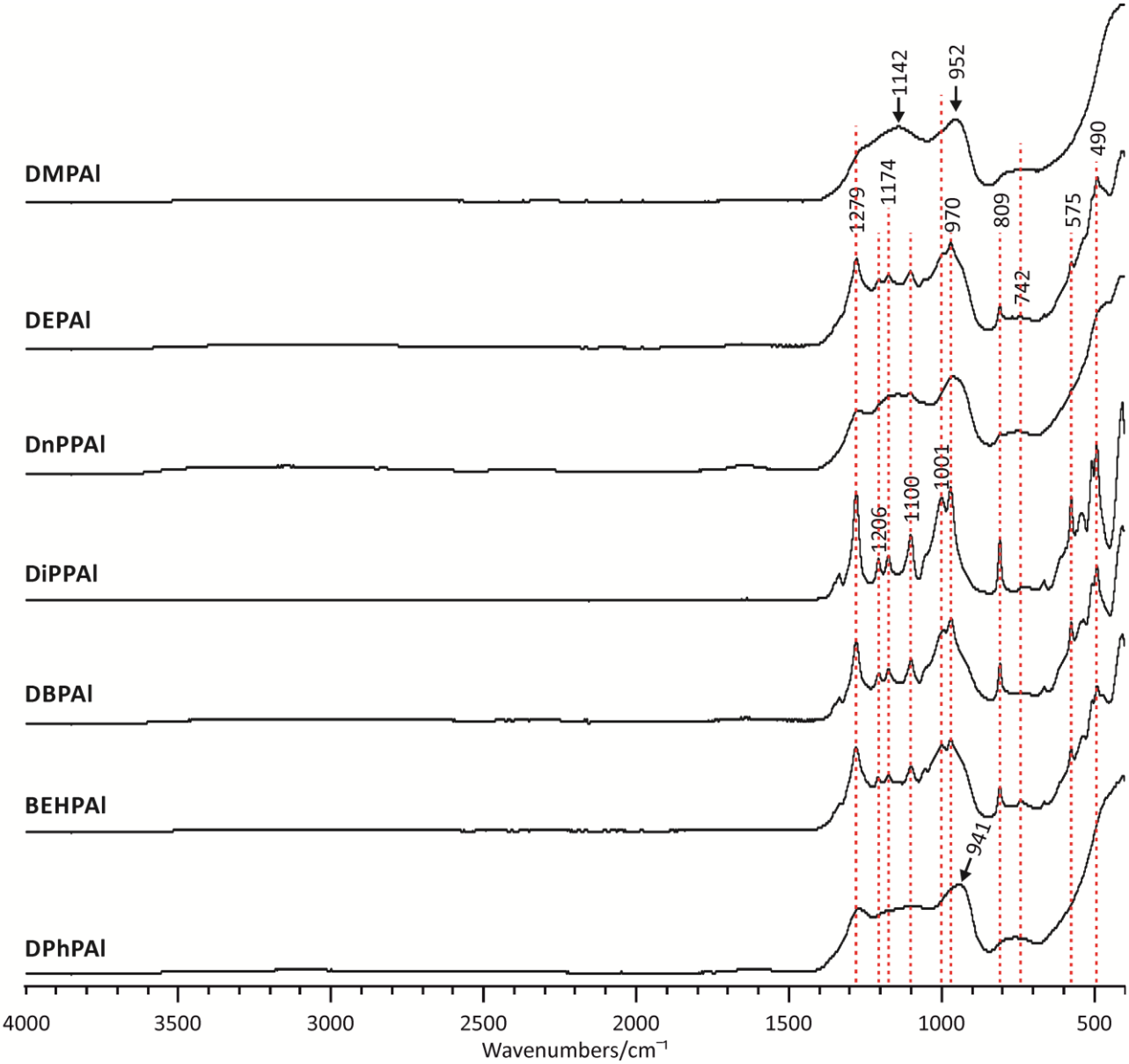

Figure S18. FTIR spectra of the solid residues from DOPAl thermal degradation carried out in air at 600 °C.

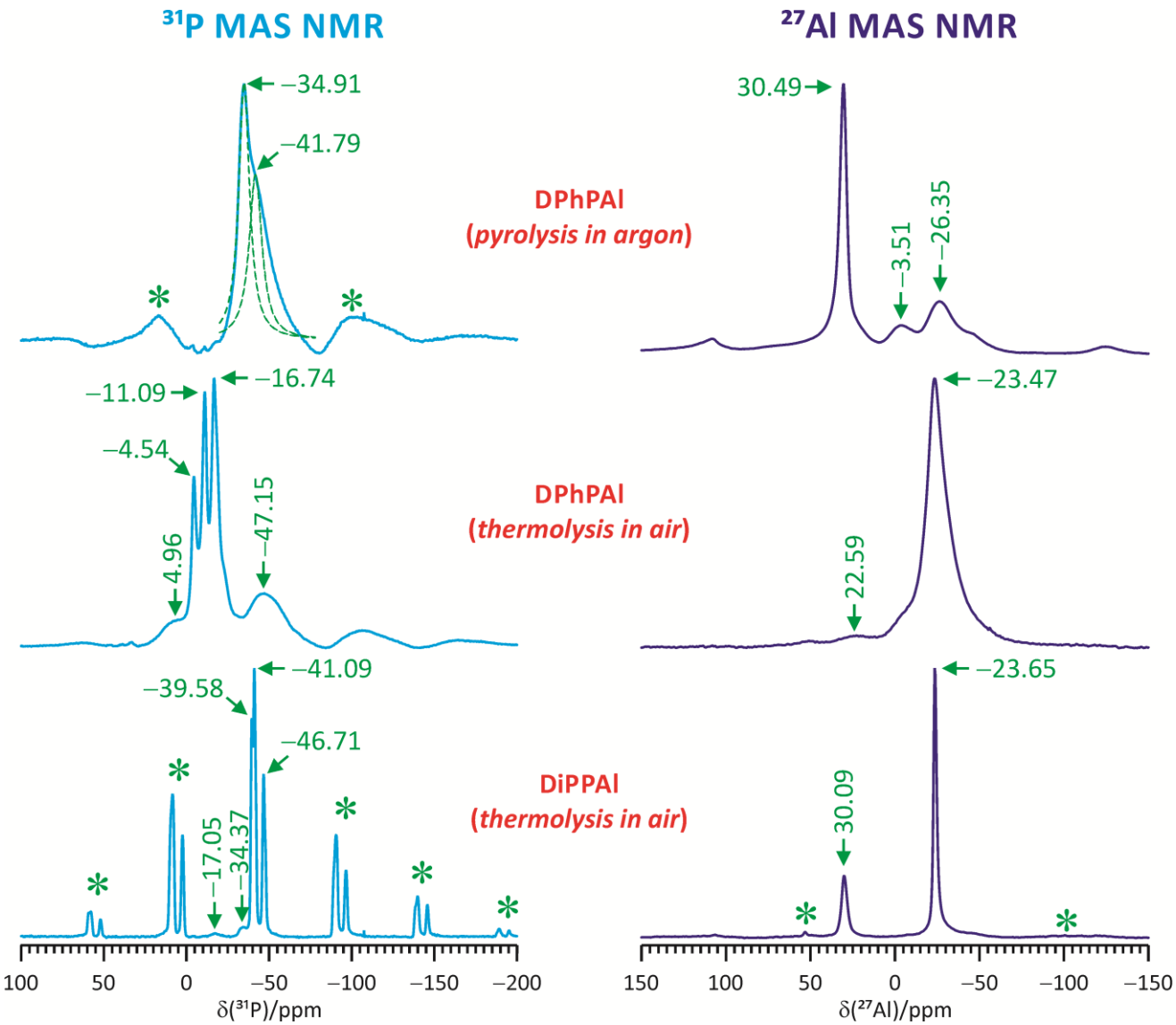

Figure S19. ^{31}P (*left side*) and ^{27}Al (*right side*) MAS NMR spectra of the solid residues from: DiPPAl and DPhPAl thermolysis carried out for 6 h in air, or DPhPAl pyrolysis conducted for 6 h in argon. Spinning sidebands are indicated with asterisks, whereas peaks fitted to the experimental spectrum are shown with green, dashed lines.

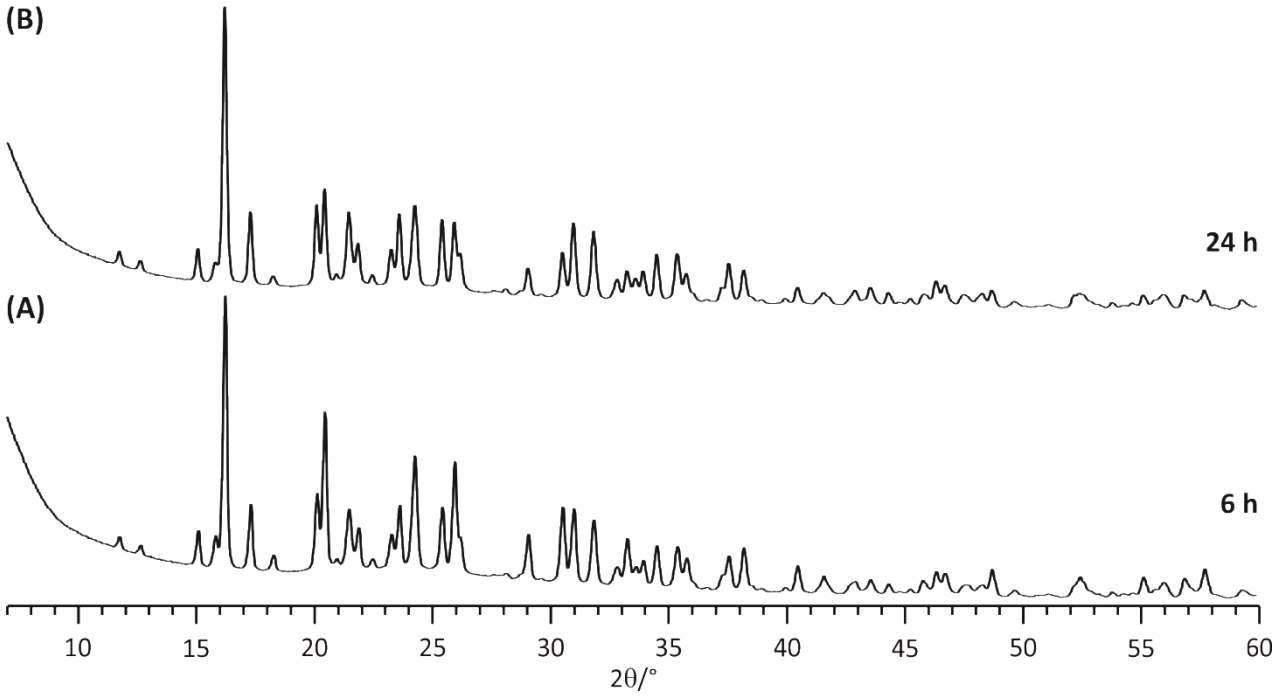

Figure S20. PXRD patterns of the solid residues obtained in the course of BEHPAl thermal degradation carried out in argon at 600 °C for: (A) 6 h and (B) 24 h.

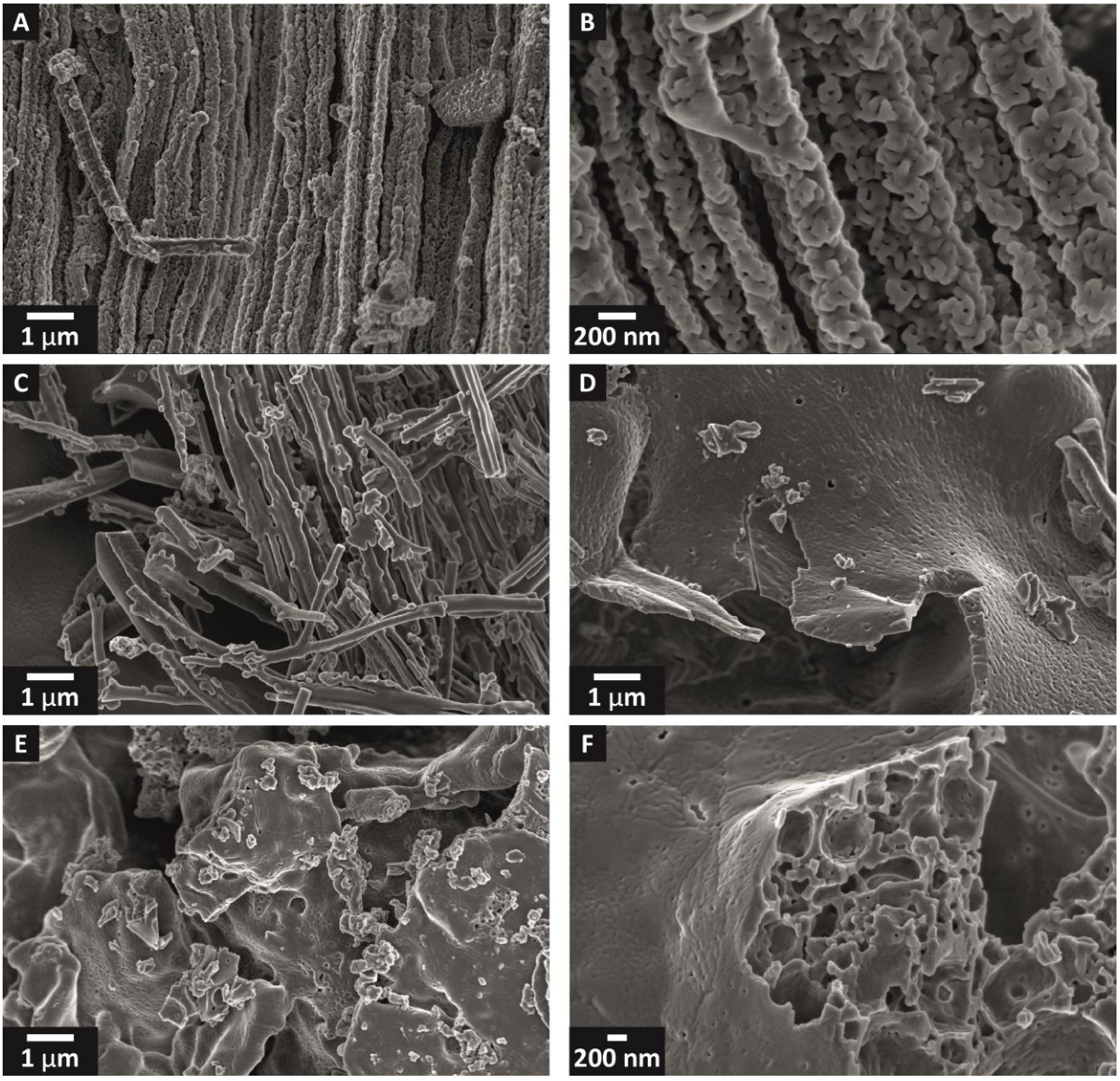

Figure S21. SEM images of the solid residues from aliphatic DOPAl thermal degradation carried out in air at 600 °C. Sample obtained from: (A, B) DnPPAl, (C, D) DiPPAl, (E, F) DBPAl.

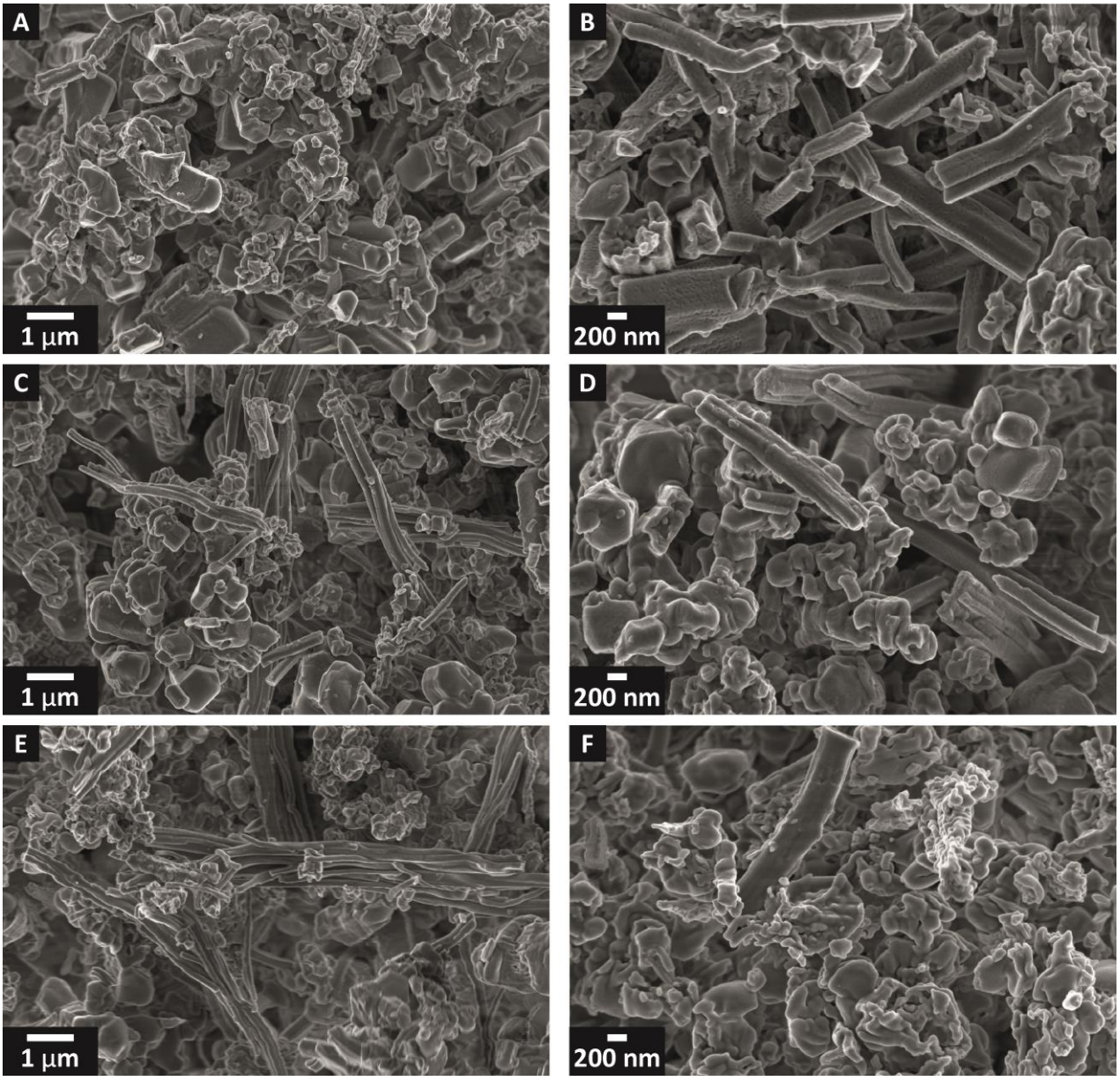

Figure S22. SEM images of the solid residues from DPhPAl thermal degradation carried out in argon (A–D) or in air (E, F) at 600 °C. For the pyrolyzates obtained in argon: sample after 24 h (A, B) or 6 h (C, D) of heating.

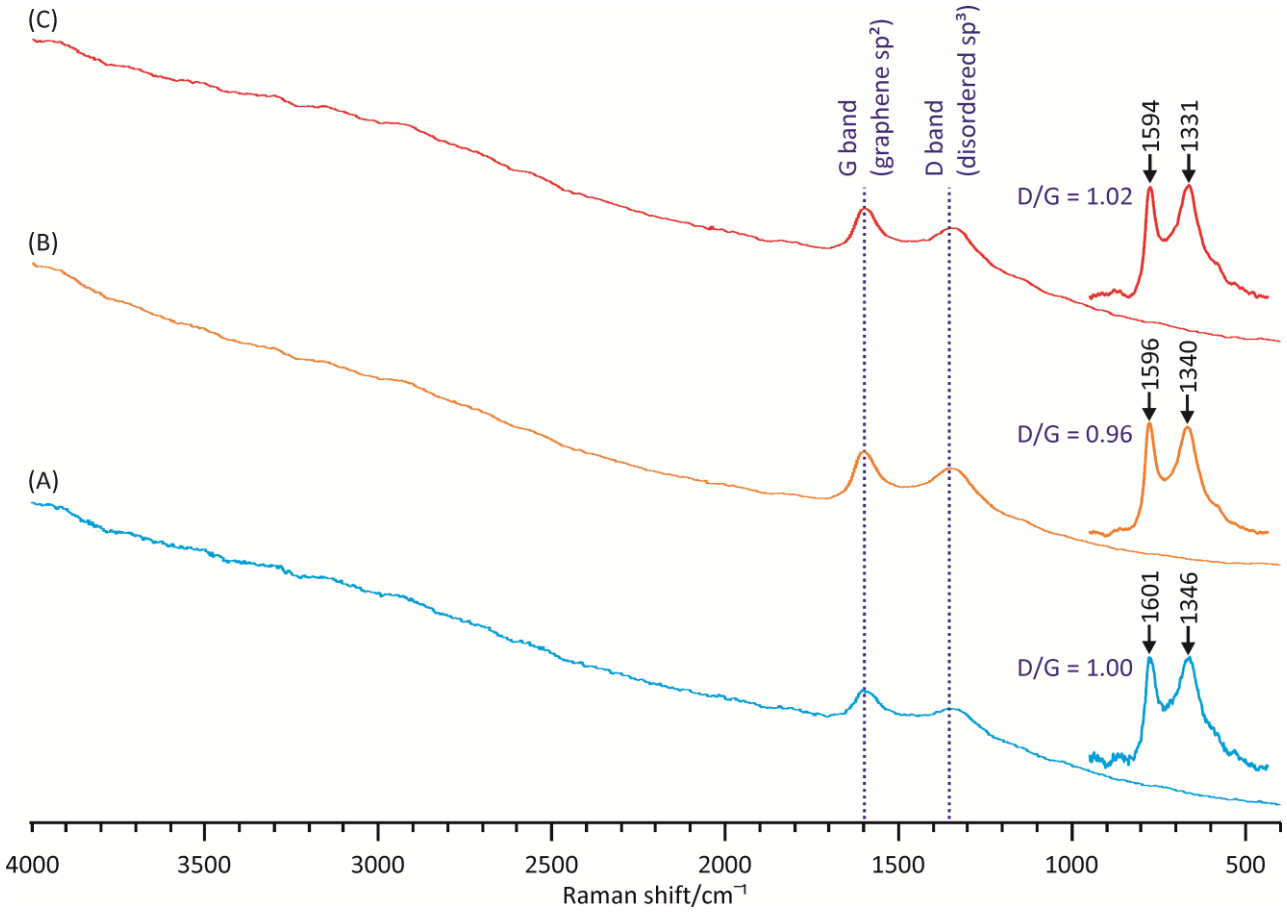

Figure S23. Raman spectra of the solid residues obtained in the course of DPhPAl thermal degradation carried out: (A) for 6 h in air at 600 °C (blue lines), (B) for 6 h in argon at 600 °C (orange lines) and (C) for 24 h in argon at 600 °C (red lines). As insets the 2000–800 cm^{-1} fragments of Raman spectra after baseline correction are presented: D/G denotes a ratio of the D band intensity to the G band intensity.